Young stellar clusters containing massive Young Stellar Objects in the VVV Survey.

J. Borissova[1,2], S. Ramírez Alegría[1,2], J. Alonso[2,3], P. W. Lucas[4], R. Kurtev[1,2], N. Medina[1,2], C. Navarro[1,2], M. Kuhn[1,2], M. Gromadzki[1,2], G. Retamales[1,2], M. A. Fernandez[1,2], C. Agurto-Gangas[1,2], A.-N. Chené[5], D. Minniti[2,6,7], C. Contreras Peña[4], M. Catelan[2,3], I. Decany[2,3], M. A. Thompson[4], E. F. E. Morales[8], P. Amigo[2,2]

[1]Instituto de Física y Astronomía, Universidad de Valparaíso, Av. Gran Bretaña 1111, Playa Ancha, Casilla 5030, Chile

jura.borissova@uv.cl

[2]Millennium Institute of Astrophysics (MAS), Santiago, Chile

[3]Instituto de Astrofísica, Facultad de Física, Pontificia Universidad Católica de Chile, Casilla 306, Santiago 22, Chile

[4]Centre for Astrophysics Research, Science and Technology Research Institute, University of Hertfordshire, Hatfield AL10 9AB, UK

[5]Gemini Observatory, Northern Operations Center, 670 N. A'ohoku Place, Hilo, HI 96720, USA

[6]Departamento de Ciencias Físicas, Universidad Andres Bello, Republica 220, Santiago, Chile

[7]Vatican Observatory, V00120 Vatican City State, Italy

[8]Max-Planck-Institute for Astronomy, Germany

ABSTRACT

The purpose of this research is to study the connection of global properties of eight young stellar clusters projected in the Vista Variables in the Via Lactea (VVV) ESO Large Public Survey disk area and their young stellar object population. The analysis in based on the combination of spectroscopic parallax-based reddening and distance determinations with main sequence and pre-main sequence ishochrone fitting to determine the basic parameters (reddening, age, distance) of the sample clusters. The lower mass limit estimations show that all clusters are low or intermediate mass (between 110 and 1800 $M_{\odot}$), the slope Γ of the obtained present-day mass functions of the clusters is close to the Kroupa initial mass function. On the other hand, the young stellar objects in the surrounding cluster's fields are classified by low resolution spectra, spectral energy distribution fit with theoretical predictions and variability, taking advantage of multi-epoch VVV observations. All spectroscopically confirmed young stellar objects (except one) are found to be massive (more than 8 $M_{\odot}$). Using VVV and GLIMPSE color-color cuts we have selected a large number of new young stellar object candidates, which are checked for variability and 57 % are found to show at least low-amplitude variations. In few cases it was possible to distinguish between YSO and AGB classification on the basis of the light curves.

Subject headings: — infrared: stars — stars: pre-main sequence — stars: variables: general — (Galaxy:) open clusters and associations: general — (Galaxy:) open clusters and associations: individual (VVV CL010, VVV CL012, VVV CL013, VVV CL059, [DBS2003] 75, [DBS2003] 93, [DBS2003] 100, [DBS2003] 130)

1. Introduction

The Vista Variables in the Vía Láctea (VVV) is one of the six ESO Public Surveys using the 4 m VISTA telescope (Arnaboldi et al. 2007), which scans the Galactic Bulge and southern Disk in five near-infrared filters (Minniti et al. 2010; Saito et al. 2010; Saito et al. 2012). The VVV data are publicly available through the VISTA Science Archive (VSA; Cross et al. 2012). Technical information about the survey can be found in Saito et al. (2012) and Soto et al. (2013). A primary goal of the VVV is to describe the numerous star clusters in its coverage area in detail, which is made possible by the infrared nature of the VVV survey, its small pixel size, and its depth, which reduce the influence of dust absorption and nebulosity in the crowded regions of the Galactic Plane. In Borissova et al. (2011), we presented a catalog of 96 new cluster candidates in the disk area covered by the VVV survey. In Chené et al. (2012) we described the methodology employed to establish cluster parameters by analyzing four known young clusters: Danks 1, Danks 2, RCW 79, and [DBS2003] 132. In Chené et al. (2013, 2015) we presented the first study of seven clusters from the Borissova et al. (2011) catalog, which contains at least one newly discovered Wolf-Rayet (WR) star, member of these clusters. Later on, we use the radiative transfer code CMFGEN to analyze the K-band spectra of these stars and to derive the stellar parameters and surface abundances for a subset of them (Hervé et al. 2016). In Ramírez Alegría et al. (2014) we presented the physical characterization of VVV CL086, a new massive cluster, found at the far end of the Milky Way bar at a distance of 11±6 kpc, and finally in Borissova et al. (2014) we reported the results of our search for new star cluster candidates projected on the inner disk and bulge area covered by the VVV survey.

In this paper we continue with analysis of star clusters, using the VVV database. We present eight Galactic young clusters, which contain Young Stellar Objects (YSOs) and/or stars with emission lines in their spectra. The main goal of this investigation is to combine

photometric data for the clusters with spectroscopy of individual YSOs to better determine the properties of both the clusters and the individual YSOs.

2. The sample

Four of the clusters in our sample are selected from the Borissova et al. (2011) catalog and the rest of the clusters are selected from Dutra et al. (2003) catalog. All of them are in the VVV disk area (Minniti et al. 2010, Saito et al. 2012), and the J, H, K_S near-infrared images are used to construct the three-color images (Fig. 1) and for photometric analysis. The coordinates of the clusters are given in Table 1. For the VVV clusters, this is the first time when the photometric and spectroscopic analysis is presented. The [DBS2003] 130 is investigated by Baume et al. (2009) and $E(B-V)$ of 2.3 mag and age of 1-2 Myr were determined using the combination between optical and near-infrared photometry; the cluster [DBS2003] 93 was mentioned as a small embedded cluster, inside the GAL322.16+00.62 Hɪɪ region by Moises et al. (2011), but no deep color-magnitude diagram was reported. The clusters [DBS2003] 75, [DBS2003] 93, [DBS2003] 100 are analyzed by Kharchenko et al. (2013) team using the 2MASS photometry (which has limiting magnitude around 14 in K_S band).

Table 1. Main parameters of the clusters in the sample.

Name	RA	DEC	l	b	E(J-K)	$(M-m)_0$	Age/Myr	Mass/M$_\odot$	Γ	Radius ′
VVV CL010 [1]	12:11:47	−61:46:24	298.261	+0.738	2.14±0.2	14.55±1.3	2.7±1.5	$(1.8\pm0.5)\cdot10^3$	-0.88±0.15	30±9
VVV CL012	12:20:14	−62:53:06	299.385	−0.228	2.0±0.3	14.1±0.7	10.0±2.5	$(1.1\pm0.4)\cdot10^2$	-1.31±0.25	37±3
VVV CL013	12:28:37	−62:58:24	300.343	−0.216	2.1±0.3	13.2±1.1	3.0±2.0	$(1.3\pm0.3)\cdot10^2$	-1.33±0.08	30±3
VVV CL059	16:05:52	−50:47:48	331.243	+1.067	3.0±0.2	15.3±1.4	20.0±3.2	$(8.3\pm2.1)\cdot10^2$	-1.09±0.24	55±8
[DBS2003] 75	12:09:02	−63:15:54	298.184	−0.785	1.5±0.2	13.6±1.3	2.0±1.0	$(8.6\pm1.8)\cdot10^2$	-1.00±0.12	72±3
[DBS2003] 93	15:18:37	−56:38:42	322.160	+0.629	2.6±0.3	11.6±0.9	20.0±5.0	$(2.5\pm0.8)\cdot10^2$	-0.95±0.09	36±4
[DBS2003] 100	16:20:26	−50:54:24	332.840	−0.590	1.1±0.1	12.78±0.8	12.0±2.5	$(5.2\pm1.1)\cdot10^2$	-1.18±0.09	80±12
[DBS2003] 130	13:11:54	−62:47:00	305.269	−0.004	2.5±0.2	13.1±1.2	3.0±1.0	$(2.2\pm0.9)\cdot10^2$	-1.13±0.34	41±11

[1] The distances derived by different methods yield very discrepant results, thus the value reported in the Table is uncertain.
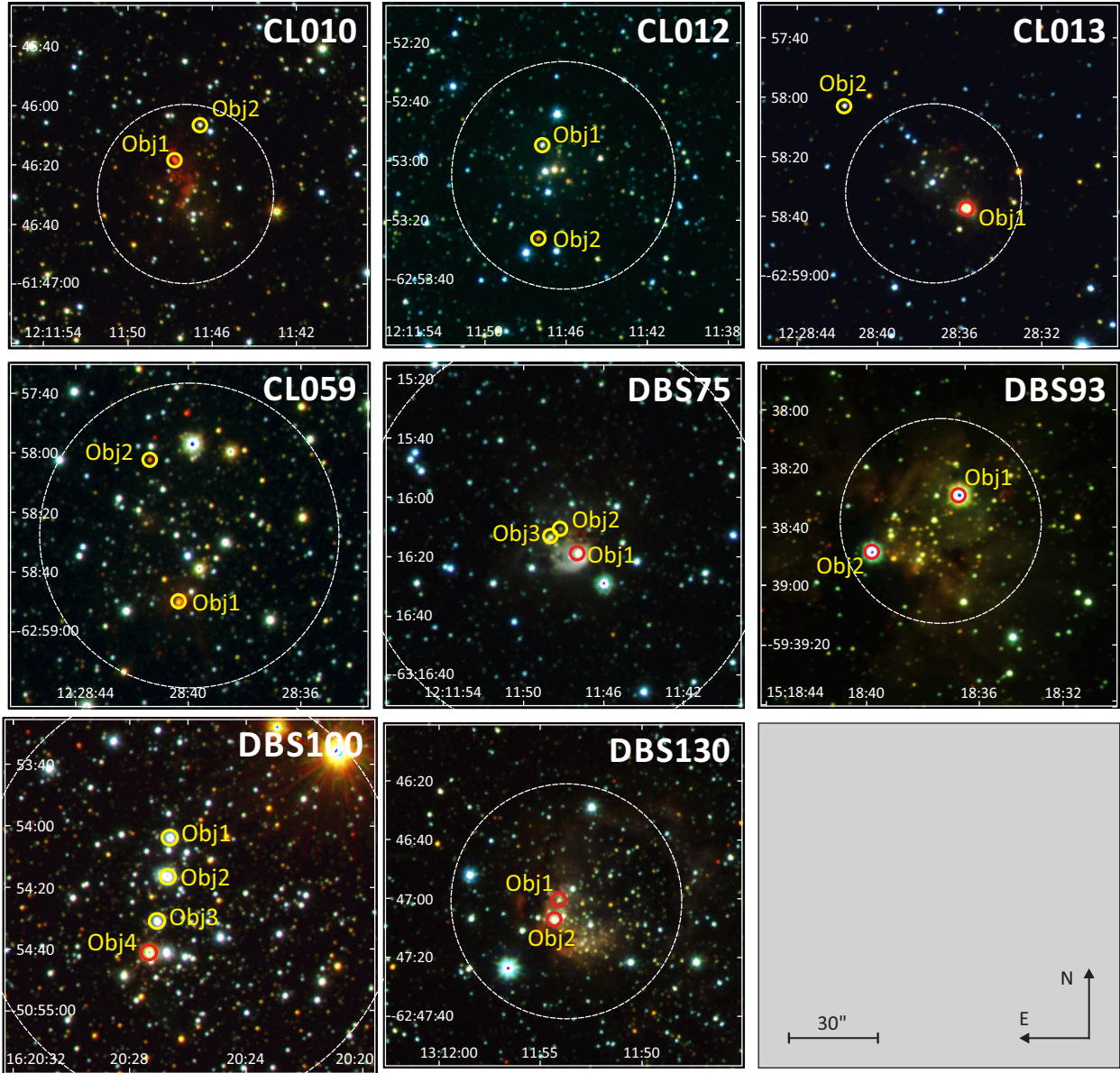
Fig. 1.— VVV JHK_S composite color images of VVV CL010, VVV CL012, VVV CL013, VVV CL059, [DBS2003] 75, [DBS2003] 93, [DBS2003] 100, and [DBS2003] 130. North is up, east to the left. The stars with emission lines in their spectra are marked.

3. The color-magnitude diagrams and fundamental parameters of the clusters.

The procedure employed for determining the fundamental cluster parameters such as age, reddening, and distance is described in Borissova et al. (2011, 2014) and Chené et al. (2012, 2013). Briefly, to construct the color-magnitude diagram we perform a PSF photometry of 10×10 arcmin J, H, and K_S fields surrounding the selected candidate. Each image was taken with 80 sec exposure time. We used the VVV-SkZ pipeline, which is an automatic PSF-fitting photometric pipeline for the VVV survey (Mauro et al. 2013) and Dophot (Alonso Garcia et al. 2015). The saturated stars (usually $K_S \leq 11.5$ mag, depending from the crowding) were replaced by 2 MASS stars (Point Source Catalog). Since 2 MASS has a much lower angular resolution than the VVV, when replacing stars we carefully examined each cluster to avoid contamination effects of crowding, using the Point Source Catalog Quality Flags given in the 2MASS catalog. To separate the field stars from probable cluster members we used the latest version of the field-star decontamination algorithm of Bonatto & Bica (2010). The algorithm divides the K_S , (H - K_S) and (J - K_S) ranges into a grid of cells. In each cell, it estimates the expected number density of cluster stars by subtracting the respective field-star number density and, summing over all cells, it obtains a total number of member stars. Grid shifts of $\pm 1/3$ the cell size are applied in each axes. The average of these is the limit for considering a star as a possible cluster member. Only the highest survival frequency after all tests were finally considered as cluster members.

We have collected spectra of 16 stars (Table 2) using the IR spectrograph and imaging camera SofI in long-slit mode, mounted on the ESO New Technology Telescope (NTT), the Infrared Spectrometer and Array Camera (ISAAC) mounted on the VLT, and the Ohio State InfraRed Imager/Spectrometer (OSIRIS) mounted on the Southern Observatory

for Astrophysical Research (SOAR) telescope.[2] The instrument set-ups give resolution of R=2200 for SofI; 3000 for ISAAC; and 3000 for OSIRIS. Total exposure times were typically 200–400 s for the brightest stars and 1200 s for the faintest. The reduction procedure for the spectra is described in Chené et al. (2012, 2013). Spectral classification was performed using atlases of K-band spectra that feature spectral types stemming from optical studies (Rayner et al. 2009; Hanson et al. 1996, 2005) in concert with the spectral atlases of Martins & Coelho (2007), Crowther et al. (2006), Liermann et al. (2009), Mauerhan et al. (2011), Meyer et al. (1998), and Wallace & Hinkle (1997). The equivalent widths (EWs) were measured from the continuum-normalized spectra using the IRAF[3] task *splot*. When the S/N was high enough, the luminosity class of the star was determined using the EW of the CO line and the Davies et al. (2007) calibration. However, for spectroscopic targets displaying low S/N it was difficult to distinguish luminosity Class I objects from their Class III counterparts. Individual extinction and distance was estimated using the spectral classifications of the objects and the intrinsic colors and luminosities cited by Martins & Plez (2006) for O type stars and by Straižys & Lazauskaitė (2009) for the rest of the spectral types (tabulated in Table 3). The uncertainties are calculated by quadratically adding the uncertainties of the photometry and the spectral classification (e.g., 2 subtypes).

The projected radius of the clusters in our sample is non homogeneously determined in the literature. Based on the much deeper VVV color magnitude diagrams with respect to the previous studies, we determined the visual radius of the clusters performing direct

[2]Based on observations gathered with VIRCAM, VISTA of the ESO as part of observing programs 179.B-2002; ESO programs 087.D-0341(A); 087.D-0490(A) and 089.D-0462(A)

[3]IRAF is distributed by the National Optical Astronomy Observatory, which is operated by the Association of Universities for Research in Astronomy (AURA) under cooperative agreement with the National Science Foundation.

Table 2. Main parameters of the observed stars in the sample.

Name	RA	DEC	J	H	K	3.6	4.5	5.8	8.0	W1	W2	W3	W4
(1)	(2)	(3)	(4)	(5)	(6)	(7)	(8)	(9)	(10)	(11)	(12)	(13)	(14)
CL010 Obj1	182.948679	-61.771908	17.18±0.20	14.87±0.14	11.07±0.20	8.37±0.30	···	6.67±0.20	···	8.41±0.02	6.16±0.02	3.62±0.01	-1.71±0.01
CL010 Obj2	182.943884	-61.768623	14.74±0.06	13.57±0.04	12.72±0.08	11.69±0.05	11.14±0.08	10.84±0.08	10.43±0.06	···	···	···	···
CL012 Obj1	185.062471	-62.882065	14.39±0.05	13.21±0.05	12.42±0.07	···	···	···	···	···	···	···	···
CL012 Obj2	185.063708	-62.890823	14.64±0.30	14.01±0.30	13.51±0.07	10.37±0.04	9.26±0.06	8.36±0.03	7.52±0.04	9.71±0.03	8.28±0.02	5.10±0.02	1.81±0.03
CL013 Obj1	187.148962	-62.976452	13.29±0.06	10.73±0.04	8.68±0.03	6.77±0.12	···	4.17±0.03	···	5.89±0.05	4.34±0.06	1.23±0.02	-1.01±0.01
CL013 Obj2	187.153946	-62.973420	15.18±0.02	13.92±0.02	12.96±0.02	···	···	···	···	···	···	···	···
CL013 Obj3	187.156037	-62.974136	13.01±0.05	12.30±0.08	11.62±0.06	···	···	···	···	11.00±0.03	10.37±0.03	7.69±0.17	6.06±0.15
CL013 Obj4	187.174247	-62.967098	14.15±0.03	13.04±0.03	12.10±0.02	10.82±0.05	10.26±0.05	9.73±0.05	8.71±0.04	6.40±0.06	6.09±0.04	2.78±0.03	0.44±0.01
CL059 Obj1	241.467897	-50.802849	15.34±0.30	13.17±0.07	10.46±0.04	7.63±0.14	6.54±0.11	5.52±0.05	4.89±0.08	7.40±0.03	5.29±0.03	1.33±0.01	-1.61±0.02
CL059 Obj2	241.472292	-50.789556	17.66±0.06	15.03±0.01	12.43±0.26	11.07±0.11	9.90±0.06	9.04±0.08	8.32±0.11	9.52±0.06	8.08±0.03	4.68±0.02	0.70±0.03
DBS75 Obj1	182.255295	-63.266605	11.79±0.08	10.53±0.07	9.10±0.06	···	···	···	···	4.08±0.08	4.01±0.03	-1.33±0.13	-4.18±0.01
DBS75 Obj2	182.258865	-63.264286	15.80±0.01	14.51±0.01	13.27±0.01	···	···	···	···	···	···	···	···
DBS75 Obj3	182.260925	-63.265038	14.45±0.01	12.75±0.01	11.29±0.01	···	···	···	···	···	···	···	···
DBS93 Obj1	229.650547	-56.641270	9.28±0.02	7.63±0.02	6.93±0.02	6.76±0.04	6.76±0.06	6.41±0.03	···	6.52±0.96	6.80±0.30	-0.54±0.35	-5.44±0.50
DBS93 Obj2	229.665245	-56.646664	8.75±0.02	8.20±0.02	8.07±0.03	7.92±0.06	8.03±0.16	···	···	···	···	···	···
DBS100 Obj1	245.111029	-50.901295	10.05±0.04	9.44±0.03	9.15±0.03	8.88±0.04	8.86±0.05	8.82±0.04	9.01±0.11	8.64±0.06	8.54±0.06	5.39±0.30	0.80±0.23
DBS100 Obj2	245.111599	-50.904770	9.49±0.04	8.92±0.04	8.58±0.03	···	···	···	···	8.15±0.04	8.15±0.06	6.13±0.58	1.34±0.20
DBS100 Obj3	245.112948	-50.908836	10.61±0.03	9.95±0.03	9.69±0.03	···	···	···	···	···	···	···	···
DBS100 Obj4	245.114143	-50.911667	11.66±0.04	9.12±0.04	7.94±0.02	···	···	···	···	···	···	···	···
DBS130 Obj1	197.975786	-62.783649	14.98±0.30	13.02±0.18	12.44±0.15	···	···	···	···	···	···	···	···
DBS130 Obj2	197.976772	-62.785511	12.51±0.05	10.87±0.06	9.81±0.04	···	···	···	···	···	···	···	···

Table 3.   Main parameters of the observed stars in the sample and Log of observations.

Name	S70(Jy)	S160(Jy)	S250(Jy)	S350(Jy)	S500(Jy)	Sp.type	M_k	$(J-K)_0$	Log
(1)	(15)	(16)	(17)	(18)	(19)	(20)	(21)	(22)	(23)
CL010 Obj1	$\cdots$	$\cdots$	247.61± 6.83	86.34±1.96	39.42±1.03	$\cdots$	$\cdots$	$\cdots$	2012-05-05T00:33:57.1361, SofI
CL010 Obj2	$\cdots$	$\cdots$	$\cdots$	$\cdots$	$\cdots$	O6-8	-3.86	-0.21	2012-05-05T00:33:57.1361, SofI
CL012 Obj1	$\cdots$	$\cdots$	$\cdots$	$\cdots$	$\cdots$	B1-2	-2.25	-0.13	2010-05-03T23:50:21.175, SOAR
CL012 Obj2	$\cdots$	$\cdots$	$\cdots$	$\cdots$	$\cdots$	$\cdots$	$\cdots$	$\cdots$	no spectra, literature YSO cand.
CL013 Obj1	136.16±10.04	72.81± 6.01	20.31± 7.39	14.17±7.43	0.00± $\cdots$	O8-B0	-3.28	-0.21	2010-05-03T00:20:35.271, SOAR
CL013 Obj2	$\cdots$	$\cdots$	$\cdots$	$\cdots$	$\cdots$	Be	$\cdots$	$\cdots$	2012-05-06T03:21:08.2385, SofI
CL013 Obj3	$\cdots$	$\cdots$	$\cdots$	$\cdots$	$\cdots$	B2-3V	-1.66	-0.11	2012-05-06T03:21:08.2385, SofI
CL013 Obj4	$\cdots$	$\cdots$	$\cdots$	$\cdots$	$\cdots$	$\cdots$	$\cdots$	$\cdots$	no spectra, literature YSO cand.
CL059 Obj1	129.37± 2.05	125.44±11.58	151.72± 6.60	62.34±3.58	29.34±2.76		$\cdots$	$\cdots$	2011-04-11T06:46:40.0196, ISAAC
CL059 Obj2	$\cdots$	$\cdots$	$\cdots$	$\cdots$	$\cdots$	$\cdots$	$\cdots$	$\cdots$	no spectra, literature YSO cand.
DBS75 Obj1	693.44±33.09	0.00:	$\cdots$	$\cdots$	$\cdots$	O7-B0	-3.86	-0.21	2011-04-17T00:20:50.0068, SofI
DBS75 Obj2	$\cdots$	$\cdots$	$\cdots$	$\cdots$	$\cdots$	$\cdots$	$\cdots$	$\cdots$	no spectra, literature YSO cand.
DBS75 Obj3	$\cdots$	$\cdots$	$\cdots$	$\cdots$	$\cdots$	$\cdots$	$\cdots$	$\cdots$	no spectra, literature YSO cand.
DBS93 Obj1	$\cdots$	$\cdots$	$\cdots$	$\cdots$	$\cdots$	$\cdots$	$\cdots$	$\cdots$	2011-04-15T03:35:36.6140, SofI
DBS93 Obj2	844.40±28.34	975.70:	$\cdots$	$\cdots$	$\cdots$	$\cdots$	$\cdots$	$\cdots$	2011-04-15T03:35:36.6140, SofI
DBS100 Obj1	$\cdots$	$\cdots$	$\cdots$	$\cdots$	$\cdots$	O4-5	-4.68	-0.21	2011-04-17T08:52:41.0839, SofI
DBS100 Obj2	$\cdots$	$\cdots$	$\cdots$	$\cdots$	$\cdots$	O7-8	-3.86	-0.21	2011-04-17T08:52:41.0839, SofI
DBS100 Obj3	$\cdots$	$\cdots$	$\cdots$	$\cdots$	$\cdots$	O6-7	-4.13	-0.21	2011-04-17T08:52:41.0839, SofI
DBS100 Obj4	$\cdots$	$\cdots$	$\cdots$	$\cdots$	$\cdots$	G2-3	-1.18	0.35	2011-04-17T08:52:41.0839, SofI
DBS130 Obj1	418.99±25.94	0.00:	$\cdots$	$\cdots$	$\cdots$	$\cdots$	$\cdots$	$\cdots$	2011-04-18T02:36:44.5824,SofI
DBS130 Obj2	$\cdots$	$\cdots$	$\cdots$	$\cdots$	$\cdots$	$\cdots$	$\cdots$	$\cdots$	2011-04-18T02:36:44.5824,SofI

star counting in the K_S band with $10''$ radius, assuming spherical symmetry. That number is then divided by the area of the rings to determine the stellar density. The projected star number density as a function of radius is shown in Fig. 2. The cluster boundary was determined by fitting the Elson et al. (1987) theoretical profile, which represents well the young clusters. The obtained values are tabulated in Table 1, where the errors are errors from the fit.

3.1. VVV CL010

VVV CL010 was selected from the star-cluster list of Borissova et al. (2011), where it is described as a reddened stellar group, superposed on the strong nebulosity of the HII region GAL 298.26+00.74. The region contains several infrared, maser and mm sources, summarized in the recent paper of Caratti o Garatti et al. (2015) as follows: the infrared source [HSL2000] IRS 1, coincident with IRAS 12091-6129, was firstly identified by Henning et al. (2000) at middle infrared (MIR) wavelengths, together with a second source [HSL2000] IRS 2, located $\sim 28''$ westwards. The HII region G298.2622+00.7391 is the dominant source at $8\,\mu$m. $L_{\rm bol}$ values from the literature range form 1.6 to $5.2 \times 10^4\,{\rm L_\odot}$ (Walsh et al. 1997; Henning et al. 2000; Lumsden et al. 2013), depending on the adopted distance (3.8–5.8 kpc). According to these estimates, the source spectral type ranges from B0.5 (Henning et al. 2000) to O8.5 (Walsh et al. 1997). Both CH_3OH (at 6.67 GHz) and OH maser (at 1.665 GHz) emissions are detected towards the source (Walsh et al. 2001). Very close to [HSL2000] IRS 1 (Cyganowski et al. 2008) observed EGO emission, namely the EGO G298.26+0.74. Outflow emission from CO (2–1) and CS (2–1) has been reported by Osterloh et al. (1997). The H_2 images of Caratti o Garatti et al. (2015), does not show any H_2 emission at the EGO position, but a well collimated jet is identified, possibly due to the presence of a multiple system. We tried to identify this multiple system on the
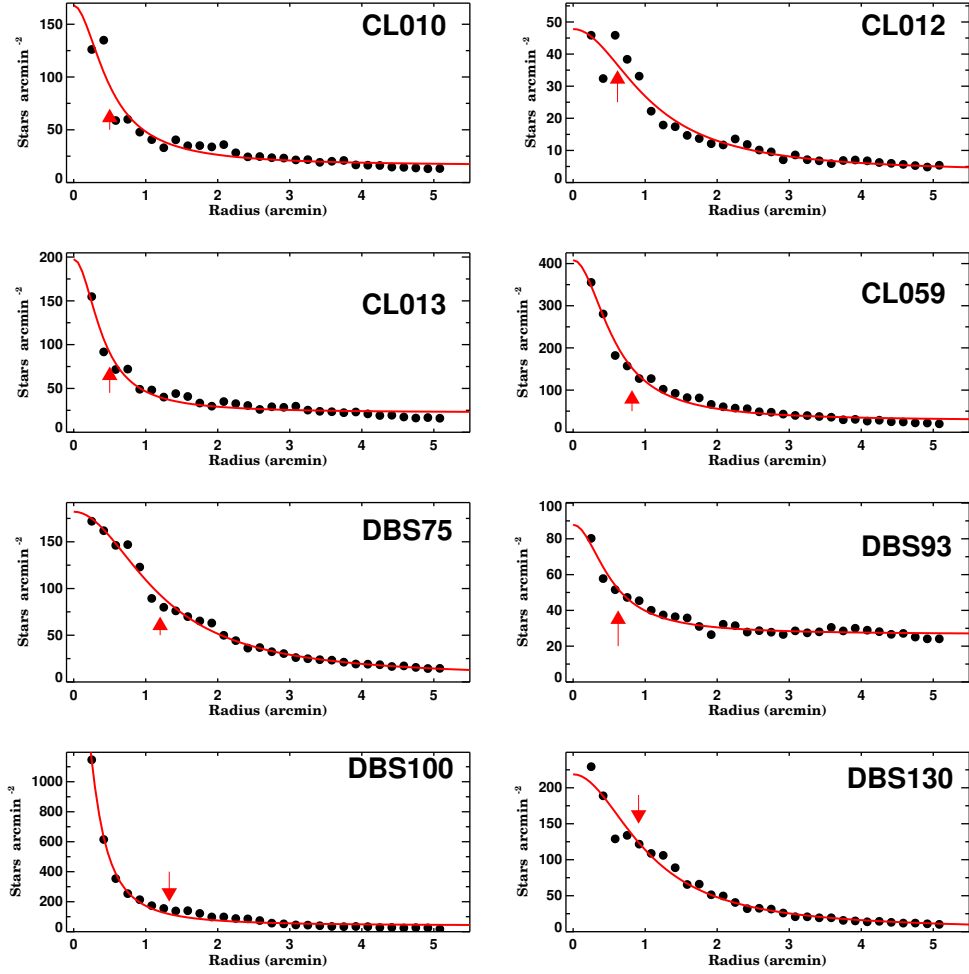
Fig. 2.— The radial density profiles as a function of radius of the clusters in our sample. The solid line stands for the best fit, the arrow marks the obtained radius of the cluster.

composed from 49 VVV images (each with a 16 sec exposure time) K_S band image. A plot of [HSL2000] IRS 1 (hereafter Obj 1) is shown in Fig. 3. As can be seen, it was not possible to resolve the object, because of the relatively large pixel size (0.339 arcsec) of the VISTA/VIRCAM detector, but the plotted contours clearly show a non stellar image profile. This may be due to a close companion or scattered light. For comparison, on the same plot we show a GLIMPSE three-color image overlaid with ATLASGAL contours of continumm emission at 870 microns from Urquhart at al. (2013), when similar elongation can be seen.

We observed Obj 1, during our SofI 2012 run, together with 2MASSJ12114653-6146070 (hereafter Obj 2, Fig. 4, lower panel). Both objects exhibit emission lines. In Obj 1, the CO v=2-0 first overtone bandhead appears in weak emission; we also detected strong H_2 emission as in Caratti o Garatti et al. (2015), the HeI lines are in absorption, and the Brγ line is not detected. Following Bik et al. (2006) the first-overtone line CO emission most probably is produced by a circumstellar disk. Obj 2 shows He I/N III and He II in emission and weak Brγ in absorption, and tacking into account its position on the CMD can be classified as O6-8e. The $(J - K_S)$ vs. K_S diagram of the region is shown in Fig. 4. The statistical decontaminated most probable cluster members form a poorly populated main-sequence (MS) and pre–main-sequence (PMS) branches. The group of stars between $(J - K_S)$ of 3.5 and 5 and K_S between 13 and 16 mag can be dusty objects along the line of sight or near infrared excess sources, which can be expected for the star forming regions affected by high levels of differential extinction. Unfortunately, only two of the possible infrared excess sources identified from the color - color diagram (G298.2584+00.7406 and G298.2663+00.7354) have GLIMPSE measurements and can be classified as YSO candidates (see Sec. 5). The spectroscopically calculated values of $E(J - K) = 2.24 \pm 0.13$ and $(M - m)_0 = 15.4 \pm 0.8$ (12±4 kpc) of Obj 2 were adopted as a first guess for establishing the cluster's reddening and distance via isochrone fitting, and
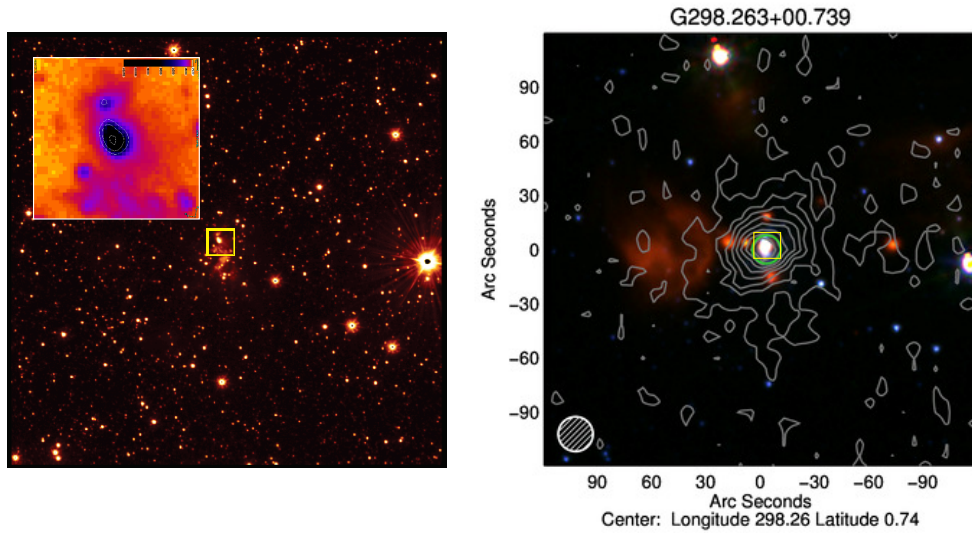
Fig. 3.— Ks band composed image of [H SL2000] IRS 1 (Obj 1). Right: A GLIMPSE three-color image overlaid with ATLASGAL contours of continumm emission at 870 microns from Urquhart at al. (2013).

improved estimates of these parameters were obtained through iterative isochrone fitting on the $(J - K_S)$ vs. K_S color-magnitude diagram. The Main Sequence (MS) isochrones for solar metallically (nearly vertical in this mass range) were taken from the Geneva library (Lejeune & Schaerer 2001) and the Pre-Main Sequence (PMS) isochrones are taken from the Pisa models (Bell et al. 2014). Starting with the spectroscopic reddening and distance estimates, isochrones were shifted along the reddening vector from their intrinsic positions until the best agreement with the observations was achieved. The stars with K_S band excesses and with large uncertainties are removed before doing the fit. The iterations were stopped when the parameters did not change. Uncertainties tied to the cluster reddening and distance were calculated by accounting for the errors of the best fit, with quadratically added photometric errors, and errors of isochrone degeneracy in K_S band for very young clusters. The green area plotted in Fig. 4 (left) shows the isochrones interval from 1 to 5 Myr, which are practically identical. For VVV CL010, a reddening and distance modulus of $E(J - K)$=2.14±0.24 and $(M - m)_0$=14.55±1.3(8.13±4.8 kpc) and age of 2.7±1.5 Myr were than adopted.

This distance is very different from the kinematic distance of 3.8-5.8 kpc obtained for Obj 1 (G298.2620+00.7394) from radial velocity measurements of CO lines (Wu et al. 2004). Following Messineo et al. (2014) we determined the Red Clump (RC) position in the 10x10 arcmin field around cluster center and calculated the RC reddening and distance modulus of 1.4 mag and 13.7 (5.56 kpc) respectively, which is close to the kinematic distance of Obj 1. Two explanations of this discrepancy are possible: since our distance was calculated using only one spectroscopic parallax, nearly vertical MS isochrone and poorly populated PMS branch, this leads to large uncertainty; and another possibility is that Obj 1 is not a cluster member. More spectroscopic observations are necessary to clarify this point.
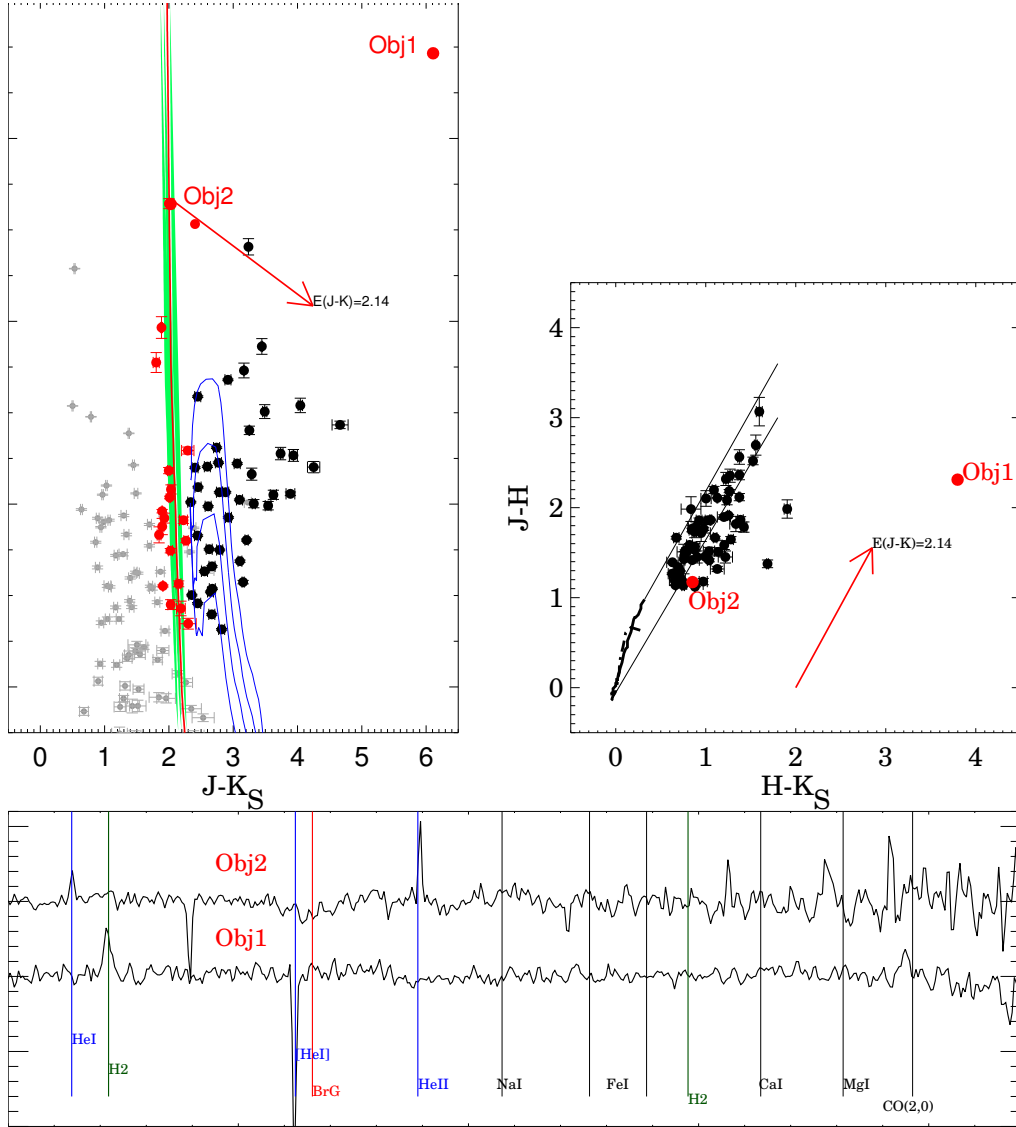
Fig. 4.— Top-left: $(J - K_S)$ vs. K_S color-magnitude diagram for VVV CL010. Gray circles are comparison field stars, red and black circles are the most probable main-sequence, PMS, and infrared excess cluster members, after statistical decontamination. Stars with spectra are denoted by red circles and are labeled. The best fit of 2.7 Myr (z=0.020) Geneva isochrone is a solid red line; the green area show the age interval between 1 and 5 Myr; while the blue solid lines stands for pre-main sequence Bell et al. (2014) isochrones for 1.0, 2.0, 4.0 and 8.0 Myr respectively. The red arrow show the reddening vector. The top-right panel shows the $(J - H)$ vs. $(H - K_S)$ color-color diagram with the reddening vector. Bottom: SofI low resolution spectra of Obj 1 and Obj 2.

3.2. VVV CL012

VVV CL012 was selected from the Borissova et al. (2011) list, where it was described as a small, embedded group containing infrared source IRAS 12175-6236. The color magnitude diagram shows stars following Main Sequence and PMS stars and few stars with infrared excess (Fig. 5), four of them are measured by Glimpse and satisfy the criterion of Class I/II objects. (see Sec. 5). The OSIRIS instrument was used to obtain a spectrum of the Obj 1. As can be seen in Figure 5, no He II line is identified in the low resolution spectra. The Paβ and Brγ lines, as well as He I are in absorption, which indicated spectral class not earlier than B2. In the H-band of the spectrum the Brackett series hydrogen lines (H I (4-13), (4-12), (4-11), and (4-10)) show weak emission, which can be formed in the surrounding circumstellar material. The EW of the Paβ and Brγ lines are consistent with B1-2 V spectral type. The combination of spectroscopic parallax values ($E(J - K) = 2.1$ and $(M - m)_0$=13.55) with the MS+PMS isochrone fitting yields a reddening and distance modulus for the cluster of $E(J - K)$=2.0±0.3 and $(M - m)_0$=14.1±0.7 (6.6±2.1 kpc) and age between 10-12 Myr. The RC distance for this field is calculated to be $(M - m)_0$=13.96±0.9 (6.2±2.7 kpc), which in this case is in good agreement with the spectro-photometric distance estimate of VVV CL012.

3.3. VVV CL013

VVV CL013 was selected from the Borissova et al. (2011) list, where it is described as a small, embedded cluster, which contains the YSO candidate [MHL2007] G300.3412-00.2190 (hereafter Obj 1; Mottram et al. 2007). The color magnitude diagram shows a relatively well populated MS and some PMS and infrared-excess stars (Fig. 6). The OSIRIS and SofI instruments were used to obtain spectra of Objs 1, 2 and 3. The spectrum of the Obj 1, shown in Fig. 6, was classified by Mottram et al. (2007) as a young stellar object
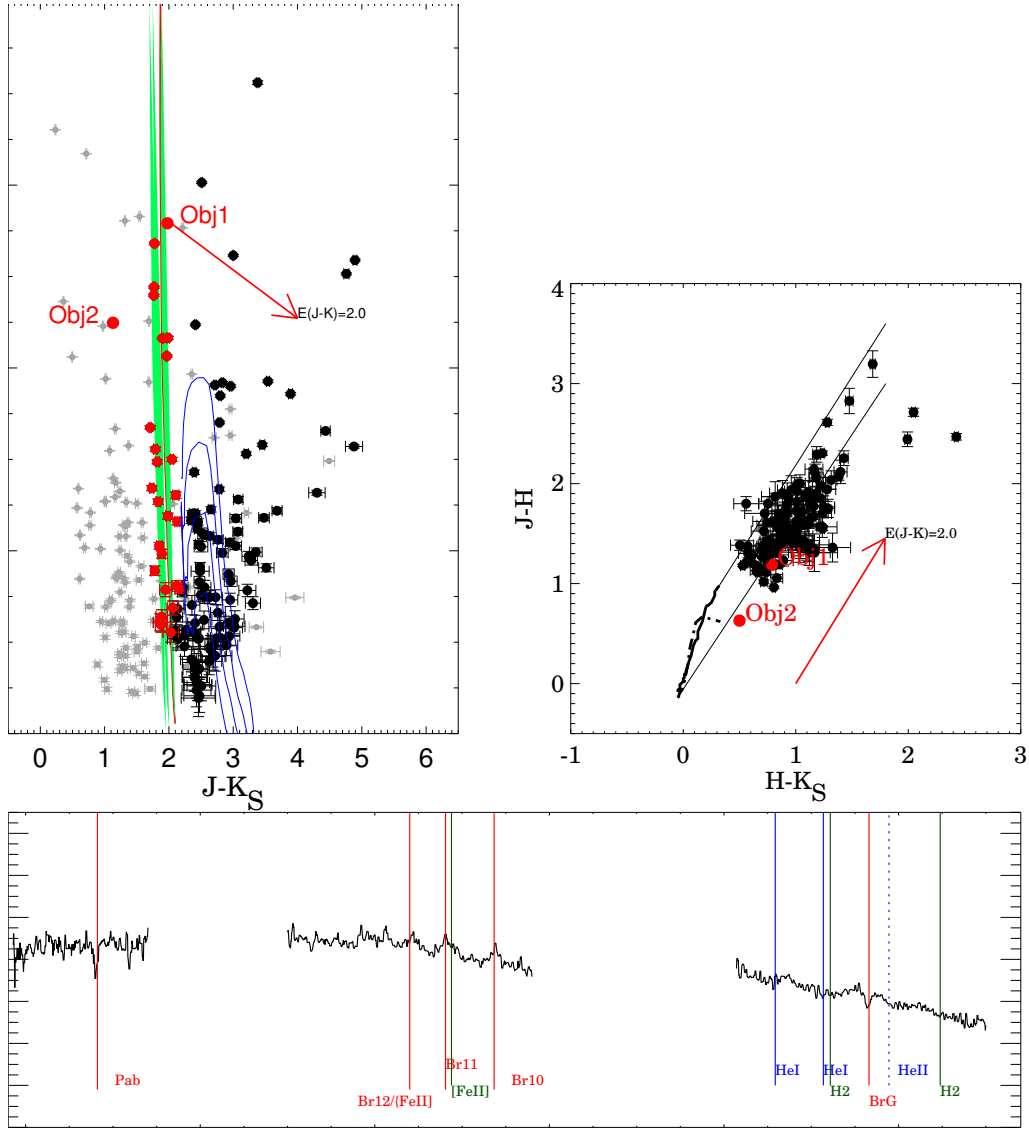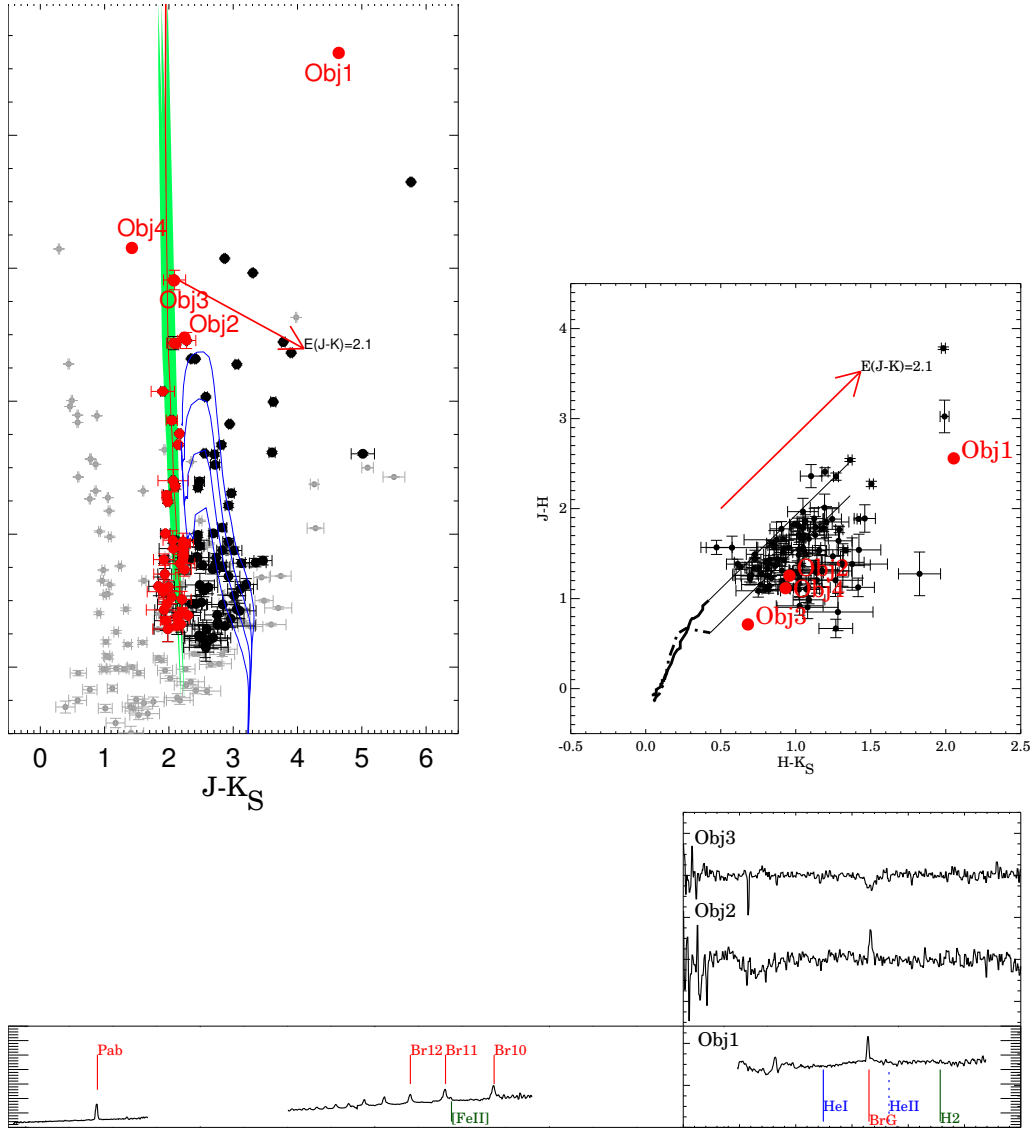
Fig. 5.— Top: $(J - K_S)$ vs. K_S color-magnitude and $(J - H)$ vs. $(H - K_S)$ color-color diagram for VVV CL012. The symbols are the same as in Fig. 4. The red solid line shows the best fit of 12 Myr Geneva isochrone. Bottom: OSIRIS low resolution spectra of Obj 1.

(YSO) candidate on the basis of 10.4 μm imaging MID-IR observations. G300.3412-00.2190 is bright, with K_S=8.68±0.03 mag and very red with $(J-K_S)$=4.61 mag. Our spectrum shows numerous hydrogen lines in emission of which Paβ and Brγ (2.17 μm) are the most prominent. Some He I lines can be identified in absorption. These atmospheric spectral features suggest for the central star a spectral type O8-B0 V. The Obj 2 shows only Brγ in emission, no other lines are identified in this region, and the object can be classified as a Be star. Obj 3 shows Brγ and He I in absorption and is most probably a B2-3 V star. Following the procedures described earlier, we calculated the reddening and distance modulus to the cluster as $E(J - K) = 2.1$±0.3 and $(m-M)_0$=13.2±1.1 (4.4±2.2 kpc) respectively. The RC distance was not calculated because of very few RC stars in the field. The best fit isochrone gives an age of 2-4 Myr. Additionally, we found in the literature a candidate YSO 2MASS J12201528-6253269 (hereafter Obj 4; Robitaille 2008). Fifteen stars were selected from our color-color diagram as stars with a possible infrared excess. Nine of them have GLIMPSE measurements and satisfy the criterion for Class I/II objects (Sec. 5).

3.4. VVV CL059

VVV CL059 was selected from the Borissova et al. (2011) list, where the high reddening of $A_V \approx 20$ mag and age between 20 and 30 Myr were determined using only photometry and isochrone fitting. Later on, Morales et al. (2013), pointed out that the cluster must be much younger than 20 Myr and determined a distance of 5.05 kpc, based on comparison with ATLASGAL images. During our ISAAC 2011 run we observed four stars—Obj 1, 3, 4, and 5—selected from the color-magnitude diagram as possible cluster members. Obj 1, 3 and 5 show well defined metal lines of Ca I (2.26μm), Mg I (2.28μm) and CO-bands, which are similar with a late-K/early-M giant spectral types, and, thus, these stars are classified as M0 III, K3-5 III, and K0-2 III, respectively (Fig. 7). However, we cannot exclude a

Fig. 6.— The $(J - K_S)$ vs. K_S color-magnitude and and $(J - H)$ vs. $(H - K_S)$ color-color diagrams for VVV CL013. The symbols are the same as in Fig. 4, the best fit isochrone is 3 Myr. Bottom: SOAR and SofI low resolution spectra of Obj 1, 2 and 3.

luminosity class I classification outright for Obj 1 and 3, which is supported by Messineo et al. (2014) Q1 and Q2 indexes. For Obj 4, on the other hand, Brγ shows emission, no H I and He II lines are detected, and a Ca I (2.26 μm) triplet shows weak emission. Given the lack of helium lines, this Obj 4 may be a B-star in formation. The statistically decontaminated color-magnitude diagram contains 73 possible cluster members and shows two evolved giant/supergiant stars (Obj 1 and 3), a well defined main sequence, and a couple of stars with infrared excess. Thirteen sources with infrared excess are identified and for 12 of them are identified as YSO candidates (see Sec. 5). Obj 5 is probably a field star based on its position on the CMD. Additionally, one high amplitude infrared variable from the Contreras Pena (2015) list is found in the field of VVV CL059. We calculated reddening and distance modulus to the cluster as $E(J - K) = 3.0\pm0.2$ and $(m-M)_0$=13.3$\pm$1.2 mag (4.6$\pm$2.5 kpc), using red giant branch classification of Obj 1 and 3. The RC distance for the field gives the same value. The best-fit isochrone gives an age of 316$\pm$38 Myr. Respectively, the supergiant classification of these objects, puts the cluster much farther at distance of 11.3$\pm$2.8 kpc, with an age of 20 Myr. According to Morales et al. (2013) CL059 is classified as still being associated with the parent molecular gas, and thus even the age of 20 Myr might be too old for this stage of evolution, considering that stellar feedback could remove the residual gas in a few Myr. Moreover, Obj 1 has diffuse warm dust/PAH emission in GLIMPSE and is associated with ATLASGAL cold dust emission, which is typical of YSOs. Our low resolution spectra, however clearly shows metal lines in absorption typical for the evolved stars. Unfortunately, there is not sufficient data (e.g., radial velocities, proper motions, high resolution spectra) to verify cluster memberships of the YSOs, to clarify the nature of Objs 1 and 3 and reveal the nature of this unusual cluster.
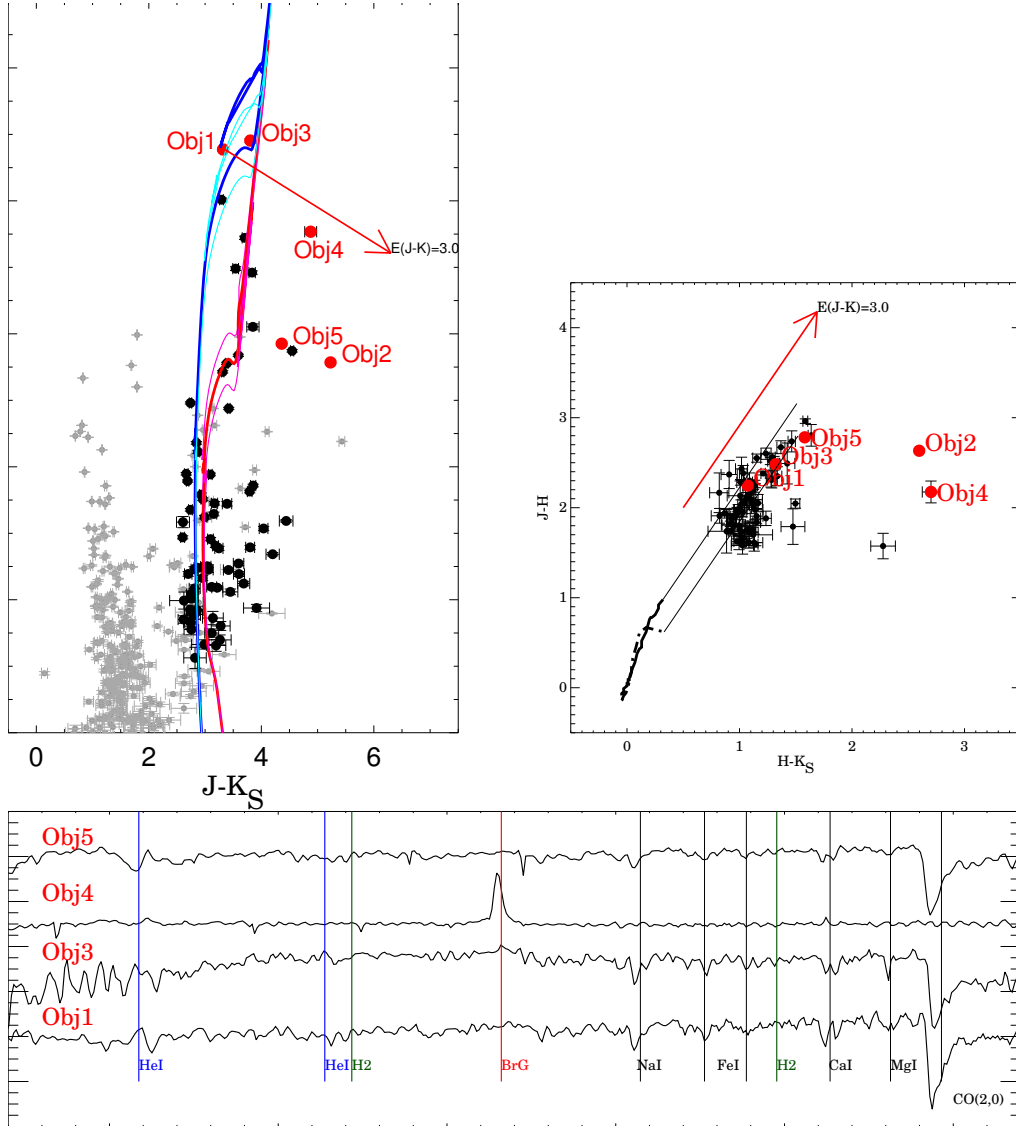
Fig. 7.— The $(J - K_S)$ vs. K_S color-magnitude, $(J - H)$ vs. $(H - K_S)$ color-color diagrams and ISAAC, VLT medium resolution spectra for VVV CL059. The symbols are the same as in Fig. 4. The best fits are for 20 Myr (blue) and 316 Myr (red).

3.5. [DBS2003] 75

The [DBS2003] 75 cluster was selected from the Dutra et al. (2003) catalog and is associated with the ESO 95-1 star-forming region and the ultra-compact HII region IRAS 12063-6256. The region was first classified as a possible planetary nebulae (Henize 1967), but latter Cohen & Barlow (1980) suggested that it is an HII region. Obj 1 (2MASS J12090127-6315597) was observed during our SofI 2011 run, and shows strong Brγ and H I 2.06μm emissions, but weak emission in He I 2.12μm. CO could be also in weak emission, but it is hard to say because this feature is at the end of the spectral range (Fig. 8). Our low resolution spectra do not allow us to determine the origin of these emission lines. Thus, it is possible that Brγ and H I 2.06μm are arising in the surrounding HII region, which is also supported by the relatively flat continuum. As pointed out by Cooper et al. (2013) the HII regions have relatively flat continua, strong H I emission, produced in an optically thin ionized region and, often, He I emission. If these emission lines arises from the HII region, than the only visible photosphere line from the YSO will be the weak emission in He I 2.12μm, which indicate early O7-B0 spectral type.

Two stars in the field are classified as YSO candidates in the literature: 2MASS J12090156-6315429 and [MHL2007] G298.1829-00.7860 (Mottram et al. 2007, hereafter Obj 2 and 3). The statistically decontaminated color-magnitude diagram (Fig. 8) contains 71 possible cluster members, nine of which were identified in the Kharchenko et al. (2013) catalog as high probability members. The main sequence is poorly populated (only 21 members), the few PMS stars and stars with IR excess are identified. Thus, dispade of relatively large cluster radius, most probably we have a very young, small stellar group, still embedded in dust and gas, rather than an evolved stellar cluster. The kinematic distance to the IRAS 12063-6256 is calculated as 10.5 kpc (Urquhart at al. 2013), the RC distance to the field is $(m-M)_0$=13.88 (5.9 kpc), while the spectroscopic distance using

the spectral classification of Obj 1 gives 1.94±0.9 kpc. The Kharchenko et al. (2013) calculated a reddening of 1.05 mag and a distance of 4.6 kpc. The best isochrone fit favors reddening and distance modulus of $E(J - K) = 1.5\pm0.1$ and $(m-M)_0=13.5\pm1.0$ (5.0±2.3 kpc) respectively. Thus, we adopted the distance to the cluster an weighted mean of all measurements as 5.6±3.0 kpc. The stellar group is young, with an age around 2 Myr.

3.6.   [DBS2003] 93

The [DBS2003] 93 cluster was selected from the Dutra el al. (2003) catalog and is associated with the RCW 92 star forming region. The color-magnitude diagram shows a couple of red giant branch stars, main sequence stars, and some stars with IR-excess (Fig. 9). Two stars were observed during our SofI, 2011 run, named Obj 1 and Obj 2. As can be seen from our low-resolution spectra, Obj 1 does not show Brγ; Mg I is in weak emission, and the CO shows a inverse P Cygni profile. The continuum declines toward the red end of the spectrum. Based on this, we conclude that this is a late M-star in formation. In contrast, Obj 2 shows shallow and broad Brγ, the metallic lines are less deep than in Obj 1 and the CO also has a P Cygni profile. Thus, the star could be a K-dwarf in formation. Both stars are identified in the Kharchenko et al. (2013) catalog and according to their proper motion analysis are cluster members. Of the cluster members identified by our decontamination, ten MS stars and two YSO candidates (DBS93 3 and DBS93 7) are also identified in the Kharchenko et al. (2013) catalog as high probability cluster members (blue circles in Fig. 9). Kharchenko et al. (2013) determined a much larger cluster radius, older age and smaller reddening. Based on our 2 magnitudes deeper CMD we determined the visual diameter of the cluster to be 0.72 arcmin. We find the reddening and distance modulus of the cluster to be $E(J - K) = 2.6\pm0.3$ and $(m-M)_0=11.62\pm0.9$ (2.1±0.87 kpc), respectively. The best fit isochrone gives an age of 20±0.5 Myr.
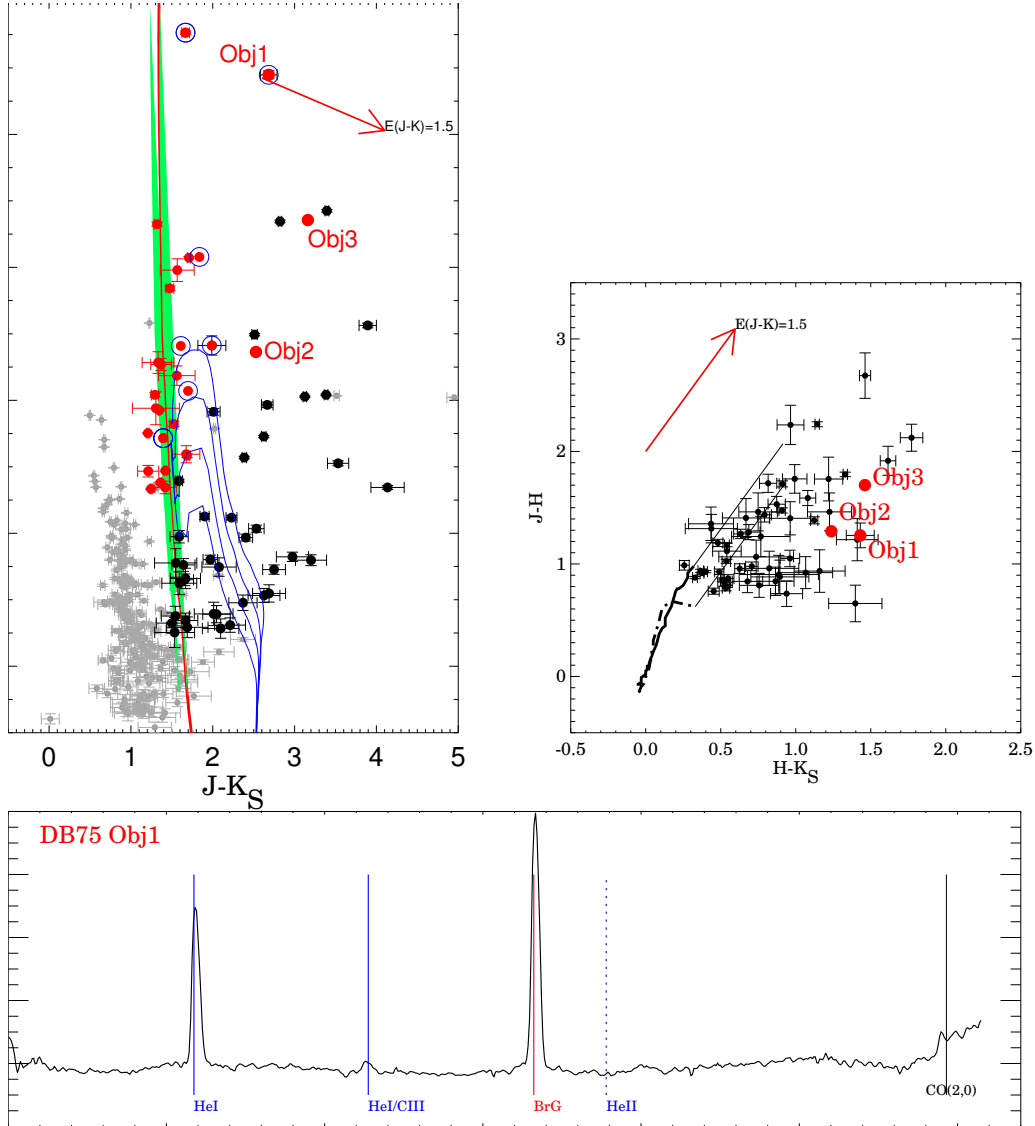
Fig. 8.— The $(J - K_S)$ vs. K_S color-magnitude diagram, $(J - H)$ vs. $(H - K_S)$ color-color diagram and SofI low resolution spectra for Obj 1 (2MASS J12090127-6315597) of [DBS2003] 75. The symbols are the same as in Fig. 4, the best fit isochrone is 2 Myr.
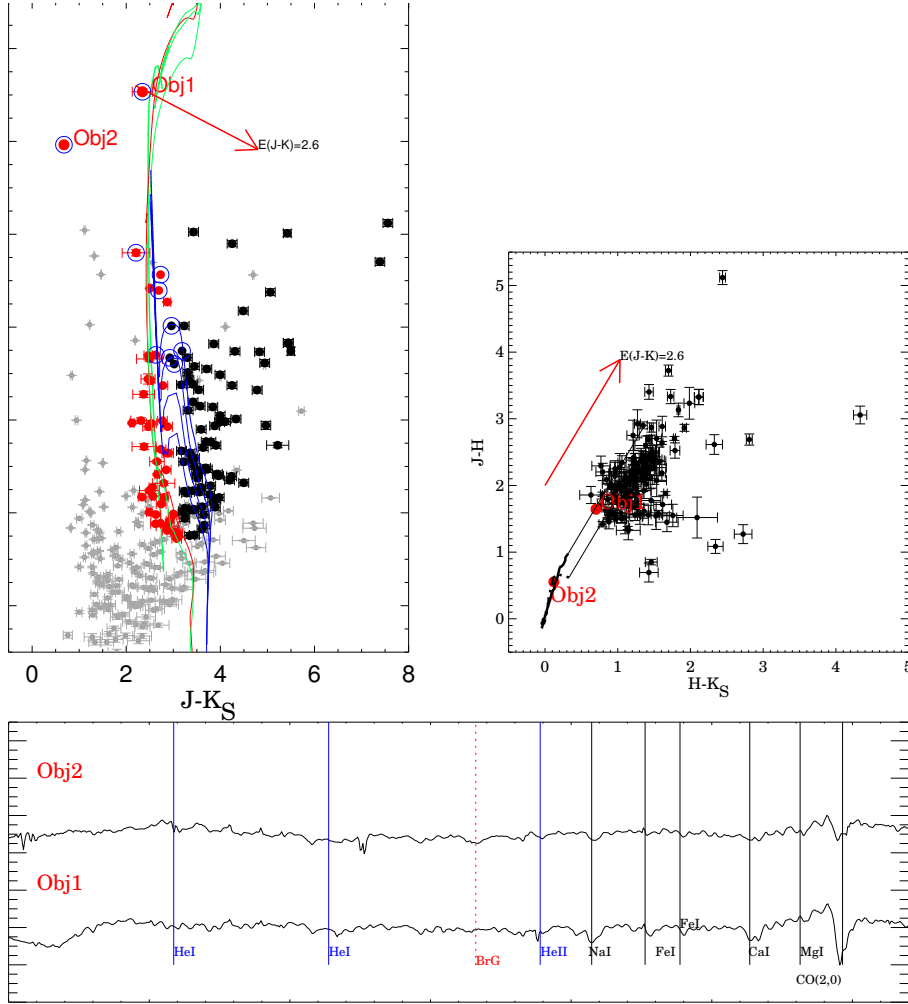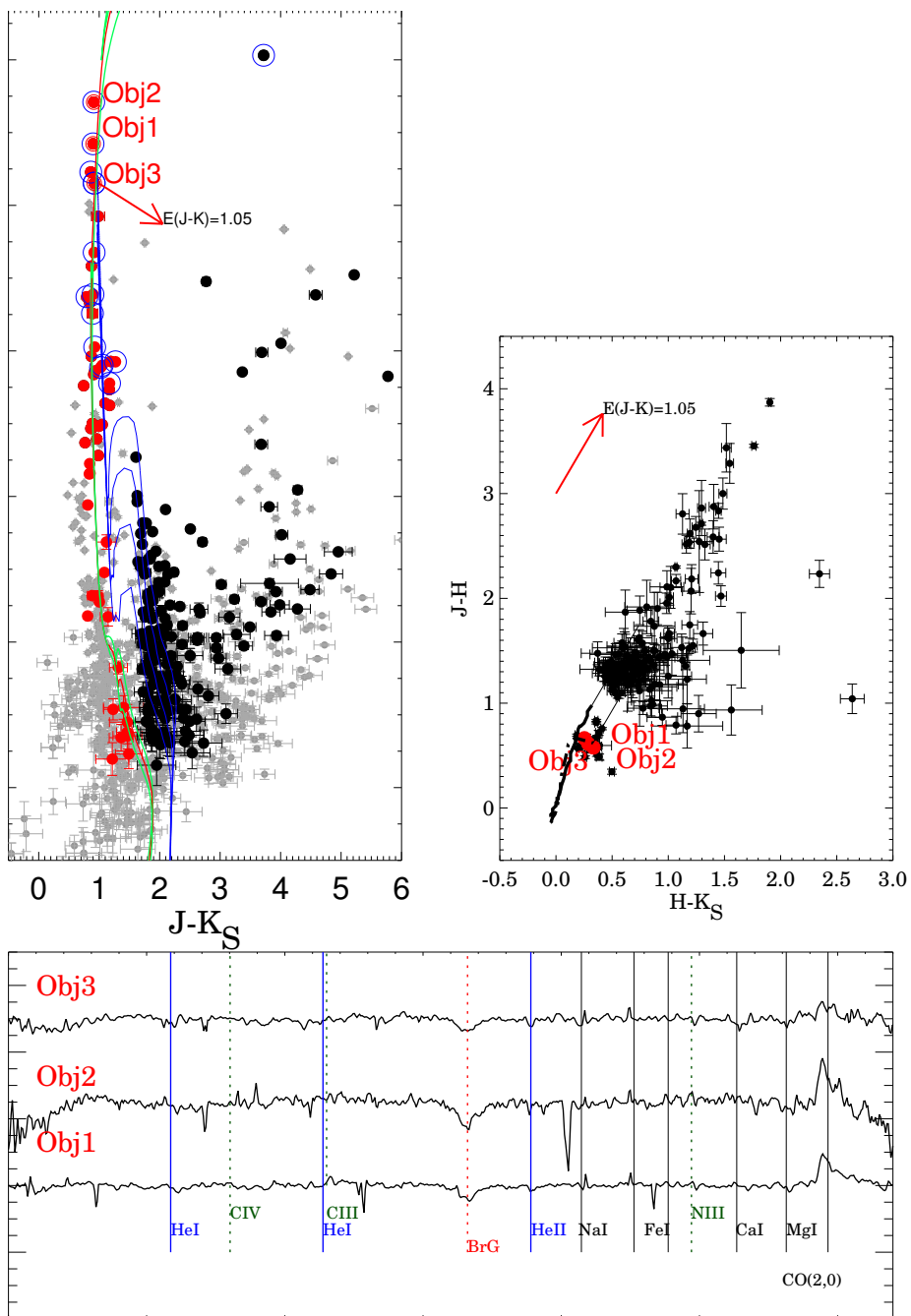
Fig. 9.— The $(J - K_S)$ vs. K_S color-magnitude diagram, $(J - H)$ vs. $(H - K_S)$ color-color diagram and SofI low resolution spectra for [DBS2003] 93. The symbols are the same as in Fig. 4, blue circles show common stars with Kharchenko et al. (2013) catalog; the best fit is 20 Myr.

3.7. [DBS2003] 100

The [DBS2003] 100 cluster was selected from Dutra el al. (2003) and is associated with the RCW 106 star forming region. The color-magnitude diagram of the cluster is shown in Fig. 10. It shows a well populated MS and a large number of PMS stars. Some stars with IR-excess can be identified in the color-color diagram (discussed in Sec. 5); two of them DBS100 ysoc9 and DBS100 ysoc10 are identified in the Kharchenko et al. (2013) catalog with high membership probability. Three stars (Objs 1, 2 and 3) were observed with SofI, during 2011 run. All of them show a rather flat continuum shape, Brγ He I and He II in absorption. Objs 1, 2 and 3 are classified as O4, O6 and O7 V spectral type, respectively. Despite their very early spectral type all three stars show CO line in emission, which can be associated with a circumstellar disk or envelope. As in the case of DBS 93 the cluster is part of Milky Way Star Cluster project (Kharchenko et al. 2013), with fundamental parameters as follows: $E(J-K)$=0.52; distance modulus of 2.2 kpc and age of 300 Myr. Our spectroscopically calculated reddening and distance modulus gives $E(J-K)$=1.1±0.1 and $(m-M)_0$=12.78±0.8 (3.59±1.3), respectively. The best fit isochrone confirm the derived spectroscopic distance and reddening and gives an age of 10-15 Myr. As in the case of [DBS2003] 93, based on our much deeper CMD, we determine this cluster to be much younger, smaller and redder than indicated in the Kharchenko catalog.

3.8. [DBS2003] 130

The [DBS2003] 130 cluster was selected from the Dutra et al. (2003) catalog and is associated with the G305 star forming region. The color-magnitude diagram of the cluster is shown in Fig. 11 and shows a well populated MS, some amount of PMS and stars with IR-excess (see Sec. 5). Two stars (Objs 1 and 2) were observed with SofI, during 2011 run. As can be seen, Obj 1 shows Brγ and He I (2.06μm) in strong emission, however, the

Fig. 10.— The $(J - K_S)$ vs. K_S color-magnitude diagram, $(J - H)$ vs. $(H - K_S)$ color-color diagram and SofI low resolution spectra for [DBS2003] 100. The symbols are the same as in Fig. 4, the blue circles represent common with Kharchenko et al. (2013) stars; the best fit isochrone is 15 Myr.

absence of He II would imply an spectral type not earlier than O8. Thus, we assign B0Ie for the spectral type of this star. The spectrum of Obj 2 is similar, but Brγ and He I are less stronger, welding to B0 Ve spectral type. The combination of spectral parallax and isochrone fit gives a reddening and distance modulus to the cluster of $E(J - K) = 2.5\pm0.2$ and $(m-M)_0$=13.1$\pm$1.2 (4.17$\pm$2.3 kpc), which is consistent with G305 region distance. The best fit isochrone gives an age of 3-5 Myr.

4.   Stellar mass of the clusters

To estimate the total cluster masses, we first constructed the cluster present-day mass function (PDMF) using the CMD and then integrated the initial mass function (IMF) fitted to the cluster PDMF. We obtained the cluster present-day mass function by projecting the main sequence most probable cluster members, following the reddening vector, to the main sequence located at the corresponding distance. The main sequence is defined by the colours and magnitudes given by Cox (2000). The slope Γ of the obtained present-day mass functions of the clusters is given in Table. 1. As can be seen, the Γ values are close to the Kroupa IMF Kroupa (2001). After deriving the cluster present-day luminosity function, using 1 K_S-mag bins, we converted the K_S magnitudes to solar masses using values from Martins et al. (2005) for O-type stars and from Cox (2000) for stars later than O9.5 V. The present-day mass functions, shown in Figure 12, are fitted and integrated between 0.1 $M_\odot$ and the most massive member candidate in each cluster. The corresponding masses are given in Table. 1, where the errors corresponds to the fitting of the IMF to the data, and includes also reddening and distance errors. All clusters in the sample are low or intermediate mass, showing masses between 110 and 1800 $M_\odot$.
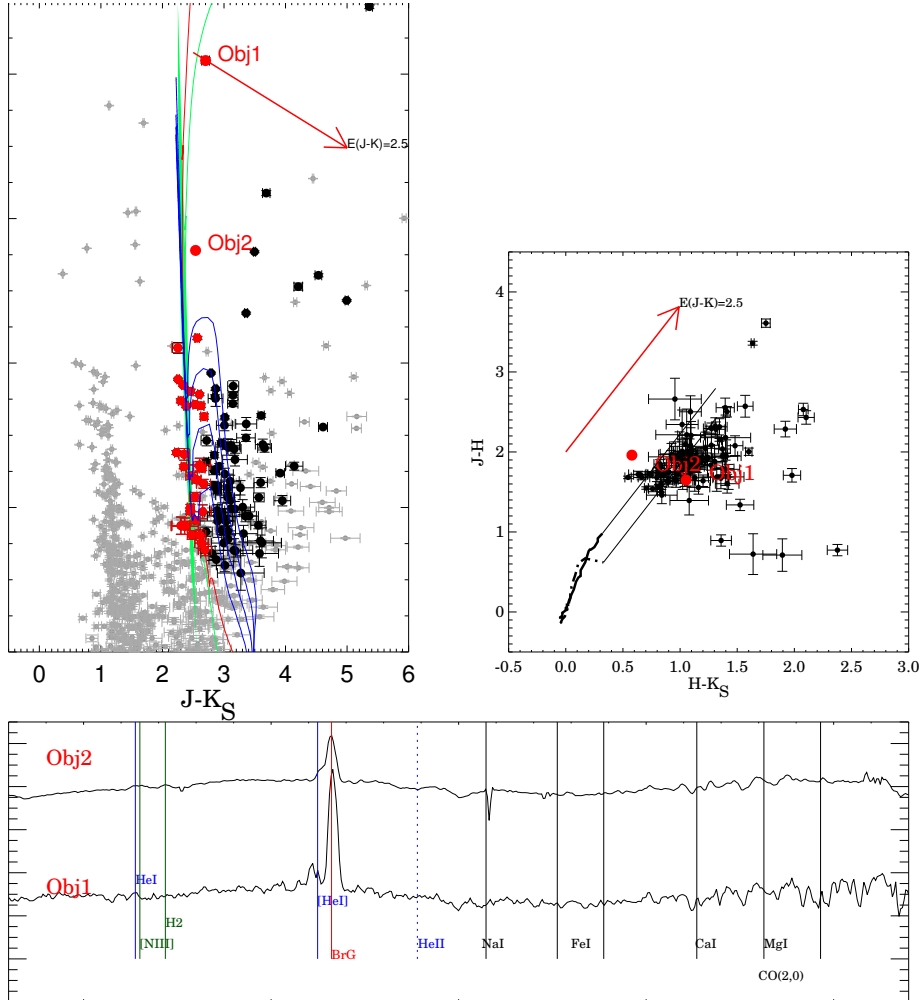
Fig. 11.— The $(J - K_S)$ vs. K_S color-magnitude diagram, $(J - H)$ vs. $(H - K_S)$ color-color diagram and SofI low resolution spectra for [DBS2003] 130. The symbols are the same as in Fig. 4, the best fit isochrone is 3 Myr.
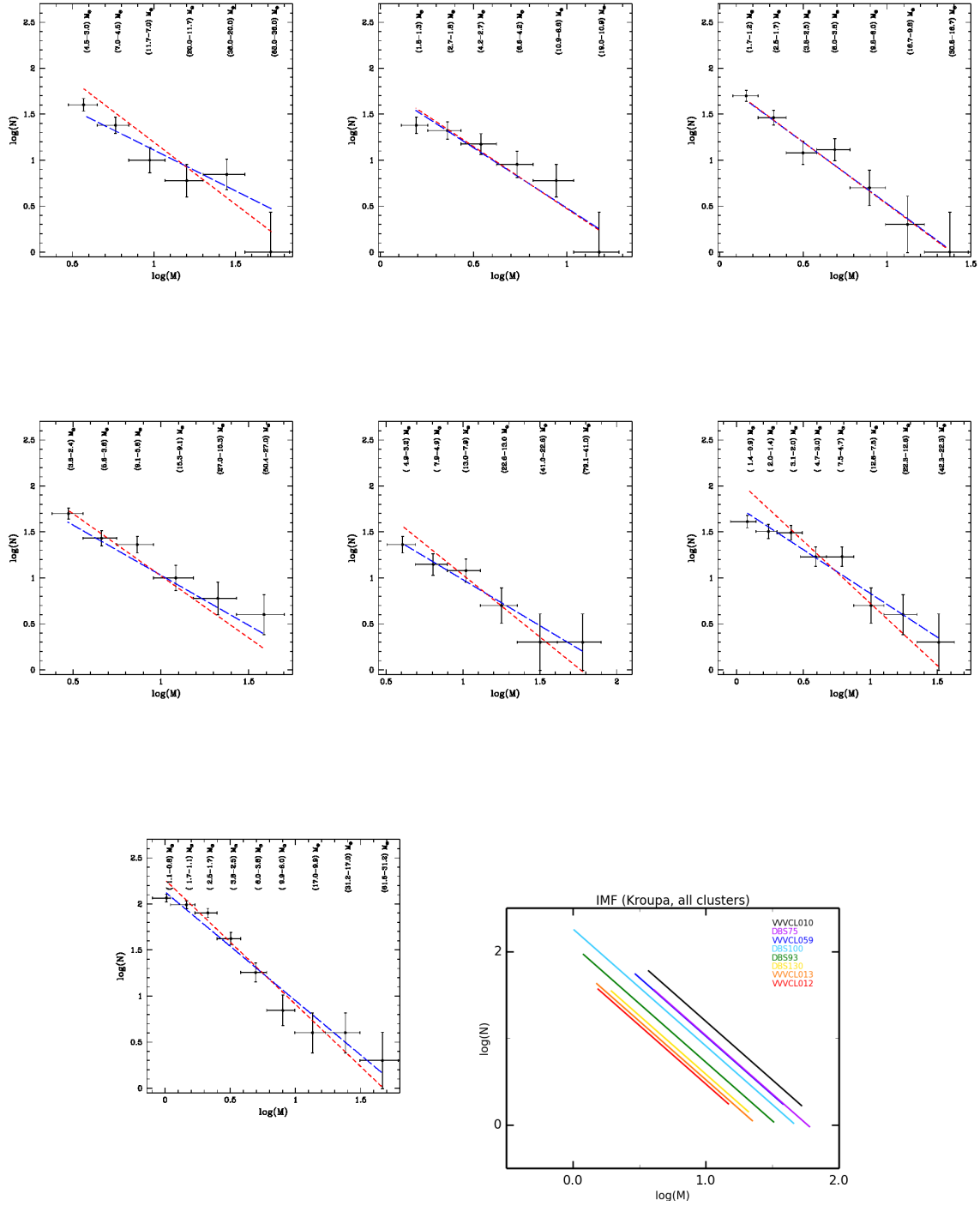
Fig. 12.— The present-day mass function of clusters from our sample: from left to right VVV CL010, VVV CL012, VVV CL013, VVV CL059 and [DBS2003] 75, [DBS2003] 93 and [DBS2003] 100.The points show the central position in the mass ranges indicated above them, and the red line corresponds to the Kroupa IMF, while the blue one stands for the best fit of the data. Bar sizes indicate the mass bin equivalent to each magnitude bin (from

5. Search for YSO candidates, variability and Spectral energy distribution

To select new YSO candidates in the studied regions we used photometric and variability criteria. First, from the near-infrared (J-H)/(H-K) color - color diagram of each cluster we selected all stars which are at least 3σ distant from the reddening line that marks the colors of dwarf stars. The list thereby obtained of 90 stars in all clusters was cross-matched with GLIMPSE measurements. Forty eight of them have photometry from GLIMPSE, and only these objects are proceeded for further inspection. Their coordinates and magnitudes are listed in Table 4 and Fig. 13 shows their $[K_S - [3.6]], [[3.6] - [4.5]]$ colors. The objects with $[K_S - [3.6]] > 0.5$ or $[[3.6] - [4.5]] > 0.5$ magnitudes are considered as a most probable class I and class II YSOs . These limits are set in order to avoid selecting objects that are more likely class III objects or normal stars (dashed red line in Fig. 13).
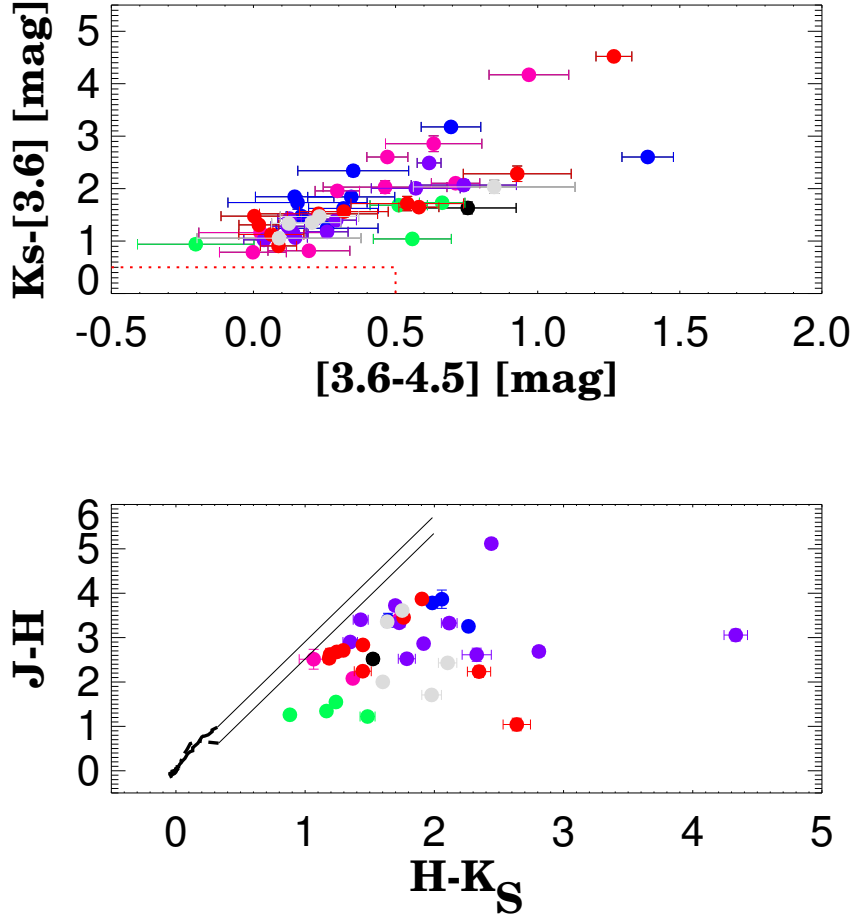
Fig. 13.— Upper panel: The $K_S - [3.6], [3.6] - [4.5]$ colour-colour plot of 48 variable stars that are detected in GLIMPSE I. The red dashed lines represent the limits used to select class I and class II YSOs. The YSO in the clusters are color-coded as follow: VVV CL 010:black; Cl 012:green; CL 013:blue; Cl 059:magenta; DBS 93:pink ; DBS 100:red; DBS 130:gray. Lower panel: The $(J - H)$ vs. $(H - K_S)$ color-color diagram of the sample. The continuous and dashed lines represent the sequence of the zero-reddening stars of luminosity classes I (Koornneef 1983) and V (Schmidt-Kaler 1982).

Table 4.   Infrared magnitudes of the YSO candidates.

Name	GLIMPSE Id.	RA	DEC	J	H	Ks	3.6	4.5	5.8	8.0
(1)	(2)	(3)	(4)	(5)	(6)	(7)	(8)	(9)	(10)	(11)
CL010 ysoc1	G298.2663+00.7354	182.956177	-61.77687	19.06±0.03	16.55±0.01	15.02±0.04	13.39±0.11	12.63±0.13	11.84±0.13	10.63±0.06
CL012 ysoc1	G299.3849-00.2418	185.054530	-62.89840	17.65±0.03	16.43±0.05	14.94±0.03	14.00±0.09	14.21±0.18	⋯	⋯ ⋯
CL012 ysoc2	G299.3948-00.2348	185.078100	-62.89268	16.55±0.01	15.29±0.01	14.41±0.02	13.37±0.08	12.81±0.11	12.00±0.20	⋯ ⋯
CL012 ysoc3	G299.3814-00.2271	185.050720	-62.88340	14.48±0.01	13.14±0.01	11.97±0.01	10.24±0.06	9.58±0.05	8.90±0.11	7.76±0.22
CL012 ysoc4	G299.3805-00.2213	185.050323	-62.87749	17.38±0.02	15.84±0.01	14.60±0.01	12.91±0.05	12.40±0.09	11.77±0.14	11.01±0.26
CL013 ysoc1	G300.3356-00.2167	187.138382	-62.97299	16.47±0.01	12.69±0.01	10.70±0.01	9.23±0.04	9.06±0.04	8.56±0.05	8.55±0.06
CL013 ysoc2	G300.3475-00.2043	187.166850	-62.96175	20.25±0.21	16.39±0.01	14.33±0.01	12.70±0.07	12.39±0.10	12.19±0.19	⋯ ⋯
CL013 ysoc3	G300.3450-00.2021	187.161850	-62.95934	19.88±0.16	16.49±0.01	14.84±0.02	13.60±0.07	13.34±0.17	⋯	⋯ ⋯
CL013 ysoc4	G300.3485-00.2288	187.164460	-62.98619	⋯	17.05±0.02	14.58±0.01	12.73±0.07	12.5±0.12	12.42±0.22	⋯ ⋯
CL013 ysoc5	G322.000+00.6165	187.143190	-62.96543	⋯	18.16±0.04	16.02±0.04	14.28±0.12	14.1±0.21	⋯	⋯ ⋯
CL013 ysoc6	G300.3240-00.1985	187.116580	-62.95386	17.41±0.02	14.16±0.01	11.89±0.01	9.29±0.06	7.90±0.07	6.96±0.03	5.95±0.02
CL013 ysoc7	G300.3290-00.2046	187.126240	-62.96040	⋯	19.70±0.13	15.57±0.03	12.39±0.07	11.70±0.08	11.28±0.08	11.47±0.14
CL013 ysoc8	G300.3420-00.2299	187.149780	-62.98669	⋯	18.14±0.05	15.48±0.03	13.64±0.09	13.30±0.13	⋯	⋯ ⋯
CL013 ysoc9	G300.3299-00.2036	187.128720	-62.95964	⋯	17.77±0.03	15.93±0.04	13.59±0.09	13.23±0.17	⋯	⋯ ⋯
CL059 ysoc1	G331.2413+01.0751	241.455527	-50.79151	16.22±0.20	13.71±0.10	12.64±0.05	11.86±0.06	11.86±0.10	11.11±0.15	⋯ ⋯
CL059 ysoc2	G331.2560+01.0600	241.489030	-50.79288	⋯	18.11±0.06	15.72±0.03	13.69±0.12	13.23±0.18	⋯	⋯ ⋯
CL059 ysoc3	G331.2624+01.0576	241.498900	-50.79050	⋯	15.27±0.04	12.80±0.02	10.84±0.05	10.55±0.06	10.19±0.09	⋯ ⋯
CL059 ysoc4	G331.2632+01.0488	241.509160	-50.79656	⋯	17.32±0.05	14.54±0.04	10.37±0.07	9.40±0.12	7.42±0.04	5.95±0.04
CL059 ysoc5	G331.2534+01.0791	241.465600	-50.78044	18.44±0.08	15.02±0.01	13.29±0.02	12.13±0.14	12.10±0.17	⋯	⋯ ⋯
CL059 ysoc6	G331.2508+01.0751	241.466740	-50.78527	⋯	15.91±0.02	12.10±0.02	9.50±0.04	9.03±0.06	8.39±0.07	8.48±0.12
CL059 ysoc7	G331.2515+01.0714	241.471480	-50.78754	⋯	17.20±0.04	13.63±0.02	10.77±0.15	10.14±0.08	9.69±0.17	⋯ ⋯
CL059 ysoc8	G331.2391+01.0533	241.476060	-50.80931	14.70±0.01	12.62±0.01	11.25±0.02	9.14±0.06	8.43±0.07	7.43±0.04	6.34±0.10
DBS93 ysoc1	G322.1434+00.6397	229.617635	-56.64518	17.32±0.10	12.20±0.03	9.76±0.03	8.33±0.03	8.20±0.03	7.70±0.02	7.78±0.06
DBS93 ysoc2	G322.1399+00.6073	229.643649	-56.67440	16.83±0.10	14.31±0.06	12.52±0.04	11.35±0.04	11.09±0.06	10.88±0.10	⋯ ⋯
DBS93 ysoc3	G322.1624+00.6065	229.679138	-56.66308	14.45±0.04	11.55±0.03	10.20±0.05	9.14±0.03	8.99±0.03	8.59±0.03	8.43±0.05
DBS93 ysoc4	G322.1493+00.6468	229.619956	-56.63598	17.98±0.10	14.93±0.09	10.59±0.02	8.10±0.03	7.49±0.03	6.87±0.03	7.06±0.10
DBS93 ysoc5	G322.1606+00.6315	229.652039	-56.64293	18.02±0.08	15.33±0.04	12.52±0.01	10.51±0.10	9.94±0.12	⋯	⋯ ⋯
DBS93 ysoc6	G322.1378+00.6453	229.603586	-56.64346	17.78±0.10	14.46±0.06	12.34±0.03	10.94±0.04	10.65±0.06	10.21±0.06	9.70±0.23
DBS93 ysoc7	G322.1834+00.6391	229.679860	-56.62423	15.40±0.08	11.68±0.03	9.98±0.03	8.82±0.03	8.69±0.05	8.33±0.05	⋯ ⋯
DBS93 ysoc8	G322.1870+00.6286	229.695662	-56.63129	16.31±0.10	12.98±0.04	11.25±0.03	9.96±0.04	9.84±0.05	9.31±0.05	8.93±0.09
DBS93 ysoc9	G322.1374+00.6164	229.631014	-56.66809	17.71±0.10	15.10±0.11	12.77±0.03	11.35±0.04	11.14±0.06	11.00±0.15	⋯ ⋯
DBS93 ysoc10	G322.1666+00.6048	229.687341	-56.66238	17.37±0.10	13.96±0.05	12.53±0.03	11.51±0.03	11.47±0.06	10.89±0.09	⋯ ⋯
DBS93 ysoc11	G322.1539+00.6228	229.650269	-56.65396	18.14±0.05	15.27±0.02	13.36±0.02	11.29±0.10	10.55±0.16	⋯	⋯ ⋯
DBS100 ysoc1	G332.8445-00.5846	245.106613	-50.89970	18.12±0.04	14.25±0.01	12.35±0.01	10.87±0.07	10.87±0.09	10.67±0.21	⋯ ⋯
DBS100 ysoc2	G332.8571-00.5875	245.123965	-50.89287	16.96±0.10	15.92±0.10	13.28±0.04	8.76±0.04	7.49±0.05	6.17±0.03	5.27±0.03
DBS100 ysoc3	G332.8418-00.5841	245.102951	-50.90125	16.17±0.01	12.72±0.01	10.96±0.02	9.65±0.04	9.63±0.06	9.27±0.06	9.60±0.11
DBS100 ysoc4	G332.8689-00.5850	245.134457	-50.88289	15.81±0.10	13.58±0.08	11.23±0.04	8.95±0.14	8.02±0.13	7.08±0.06	5.71±0.04
DBS100 ysoc5	G332.8482-00.5897	245.116364	-50.90090	18.19±0.07	15.36±0.02	13.91±0.02	12.39±0.10	12.16±0.18	⋯	⋯ ⋯
DBS100 ysoc6	G332.8383-00.5887	245.104156	-50.90699	15.90±0.01	13.19±0.01	11.90±0.01	10.77±0.09	10.71±0.07	10.46±0.08	⋯ ⋯
DBS100 ysoc7	G332.8399-00.5876	245.105026	-50.90490	19.23±0.10	16.55±0.02	15.31±0.03	13.59±0.13	13.05±0.15	⋯	⋯ ⋯
DBS100 ysoc8	G332.8347-00.5848	245.095718	-50.90691	17.95±0.14	15.34±0.02	14.14±0.01	12.58±0.10	12.26±0.12	⋯	⋯ ⋯
DBS100 ysoc9	G332.8395-00.5964	245.114143	-50.91167	11.66±0.04	9.12±0.04	7.94±0.02	7.03±0.04	6.94±0.05	6.58±0.03	6.57±0.03
DBS100 ysoc10	G332.8716-00.5631	245.113112	-50.86538	15.71±0.09	13.47±0.05	12.02±0.04	10.37±0.05	9.79±0.05	9.12±0.04	7.63±0.06
DBS130 ysoc1	G305.2451+00.0056	197.921080	-62.77509	14.43±0.05	10.82±0.03	9.07±0.03	7.73±0.04	7.61±0.04	7.16±0.02	7.05±0.06

All available K_S magnitude in VISTA Science Archive (VSA) Data Release 4 (DR4, four year database, up to 30 September 2013, http://horus.roe.ac.uk/vsa/index.html) with grades A and B (e.g. observed within optimal sky conditions) are retrieved to check the variability of the above selected YSO candidates, together with spectroscopically confirmed candidates. The level of variability seen in normal, non-variable stars is estimated to be below 0.1 mag at 12<Ks<16 using apermag3 (2″ diameter aperture) in the tile catalogs, but we put a 0.2 mag conservative limit marking the errors of the photometry and transformation to the standard system. The saturated stars, the objects with close companions (blending) and those with large photometric errors, 10 in total are removed. To analyze the rest of them we compute a set of variability indexes, namely Stetson J and K indexes (Stetson 1996), the η index (von Neumann 1941), the chi square test χ^2 (Rebull et all. 2015), the Small Kurtosis κ (Richards et al. 2011) and $\frac{\mu}{\sigma}$ (e.g. the ratio between the average K_S magnitude from light curve over the standard deviation of the data). Then we used an Unsupervised Clustering Algorithm, which identify patterns among the values of these indexes, separating populations of objects with similar features. Thus, two groups of objects are defined, one with significant amplitudes (in general, greater than 0.2 mag in K_S), which shows long and short term variability in the time domain, and another group of sources that the variability is not very significant, can be confused with noise and thus is uncertain.

Table 4—Continued

Name	GLIMPSE Id.	RA	DEC	J	H	Ks	3.6	4.5	5.8	8.0
(1)	(2)	(3)	(4)	(5)	(6)	(7)	(8)	(9)	(10)	(11)
DBS130 ysoc2	G305.2646-00.0050	197.965347	-62.78419	18.13±0.02	14.77±0.01	13.13±0.01	12.08±0.11	11.99±0.27	⋯	⋯	⋯	⋯
DBS130 ysoc3	G305.2530+00.0034	197.938602	-62.77666	17.32±0.05	14.89±0.07	12.79±0.02	11.32±0.09	11.08±0.10	⋯	⋯	⋯	⋯
DBS130 ysoc4	G305.2845-00.0122	198.010098	-62.78972	15.33±0.05	13.63±0.07	11.65±0.03	10.30±0.07	10.09±0.08	9.59±0.07	⋯	⋯
DBS130 ysoc5	G305.2641+00.0009	197.963330	-62.77818	18.33±0.04	16.33±0.01	14.73±0.03	12.69±0.12	11.85±0.26	⋯	⋯	⋯	⋯

Fig. 14, Fig. 15 and Fig. 16 show examples of MJD vs. K_S magnitudes for the non variable and variable stars, respectively. According to our analysis 57 % of the YSO candidates show signatures of infrared variability. Most of the variable stars in our sample show amplitude variations between 0.2 and 0.5 mag, and only six stars have higher amplitudes. Actually, CL059 Obj2 was taken from the Contreras Pena (2016) list of high amplitude variables, and according to SIMBAD the object CL013 ysoc6 (2MASS J12282798-6257139) is a YSO candidate; DBS100 ysoc2 (2MASS J16202975-5053343) is an AGB candidate; DBS100 ysoc4 (2MASS J16203226-5052584) is a YSO candidate in the list of intrinsically red stars in the Robitaille et al.(2008) paper. We try to determine some periods using different statistic methods, unfortunately, this was not possible on the base of the existing epochs. Nevertheless, according to the light curves and the position in the color-magnitude diagrams, we consider that the stars CL013 ysoc6; DBS100 ysoc2; DBS100 ysoc4 and DBS130 ysoc5 are most probably semi-regular asymptotic variable stars. It is well known (Robitaille et al. 2008) that the color-cut photometric selections alone can not distinguish between YSO and AGB stars. However, as we show above, the combination with infrared variability analysis can help to solve this problem.

To model the Spectral Energy Distributions (SED) of the YSO candidates we use the spectral energy distribution models of young stellar objects developed by Robitaille et al. (2008). We have collected existing measurements of these objects, from the VVV, 2MASS, GLIMPSE, WISE and HIGAL catalogs. The respective reddening and distances of each object are determined by photometry and spectroscopy in the Sect. 3, however due to their large uncertainties, we considered all models that lie within a 5 σ of the respective errors. The Robitaille models never give a single result, rather, they give a range of models and a chi-squared parameter, an example is shown in Fig. 17 for CL012 Obj2. The range of models that give an acceptable chi-squared is usually up to 5 models starting from the best fit model in our case, since the HIGAL magnitudes constrains the longer wavelength range.
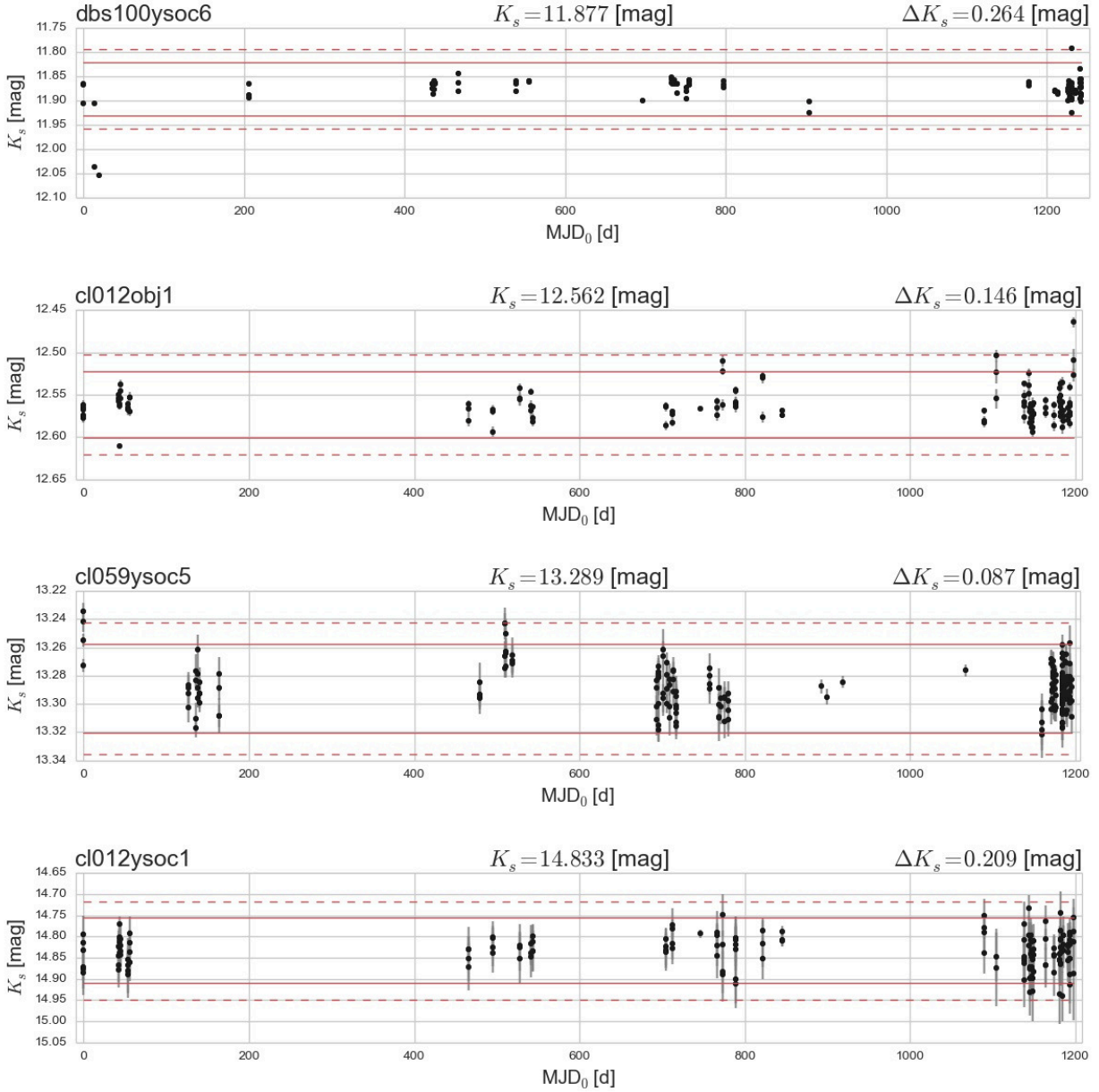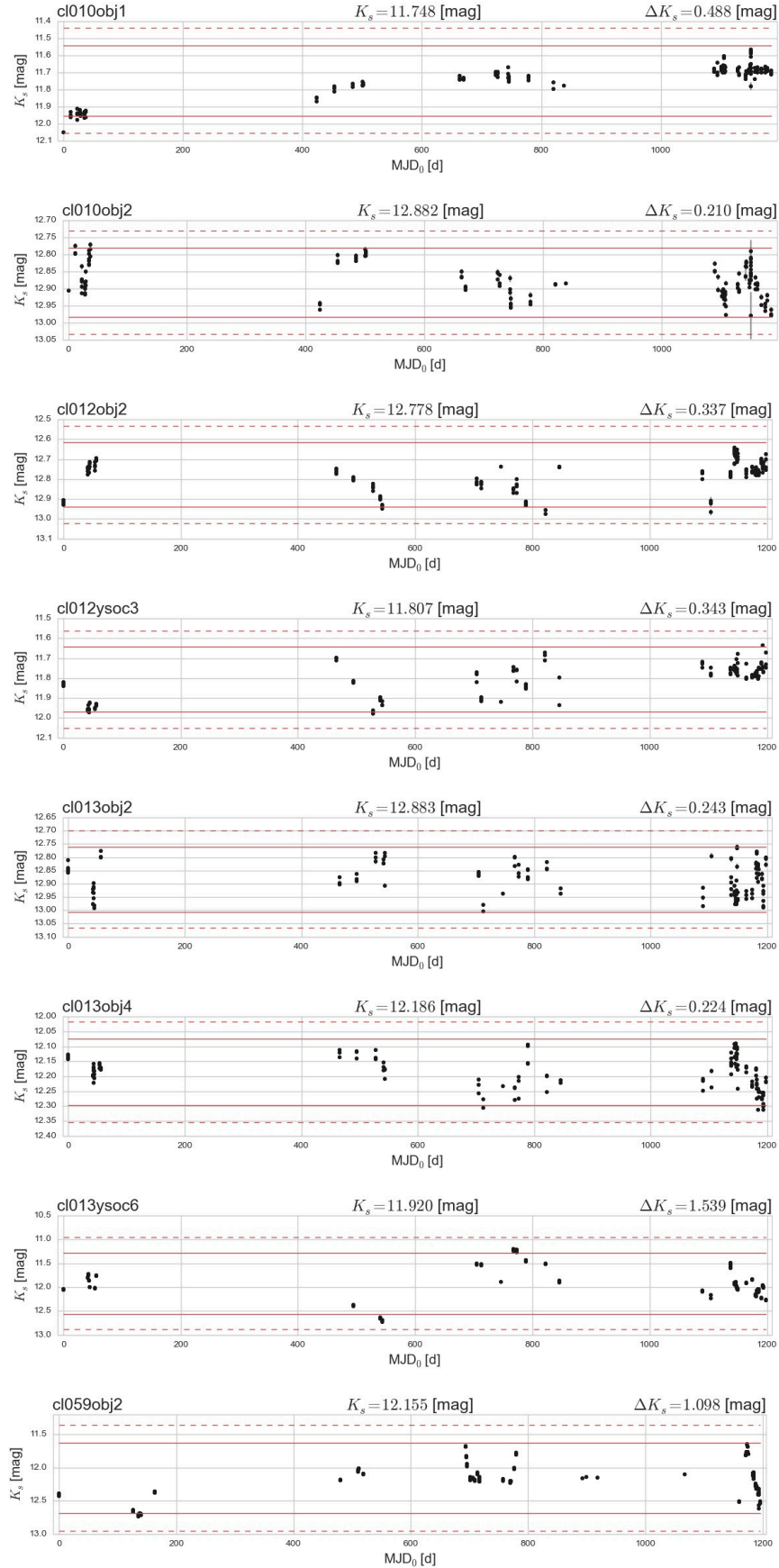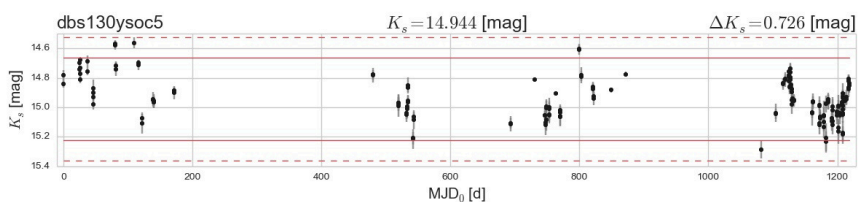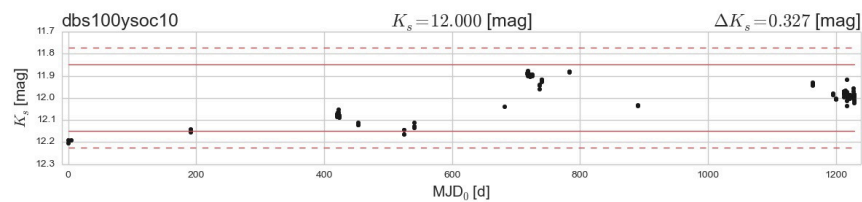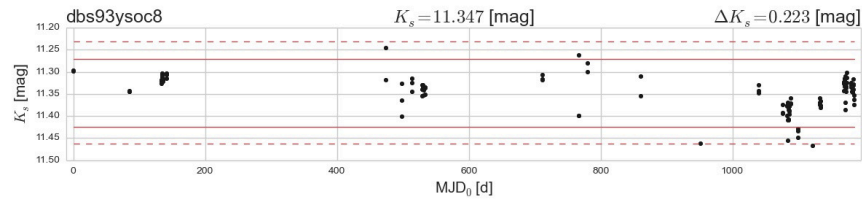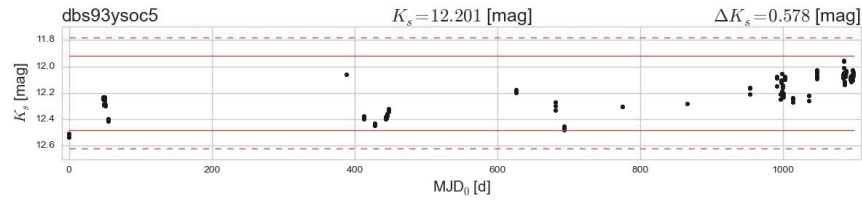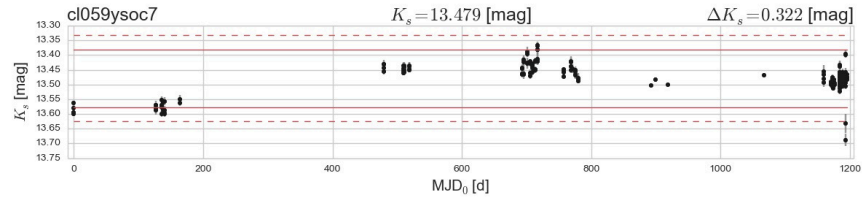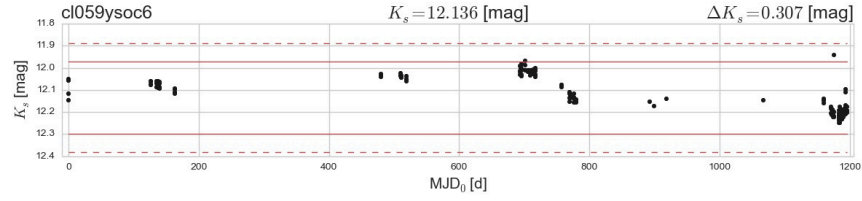
Fig. 14.— Examples of K_S magnitude vs MJD of non variable YSO candidates. The solid and dashed red lines mark the 2 and 3 σ dispersion the light curve, respectively.

cl010obj1 $K_s = 11.748$ [mag] $\Delta K_s = 0.488$ [mag]

cl010obj2 $K_s = 12.882$ [mag] $\Delta K_s = 0.210$ [mag]

cl012obj2 $K_s = 12.778$ [mag] $\Delta K_s = 0.337$ [mag]

cl012ysoc3 $K_s = 11.807$ [mag] $\Delta K_s = 0.343$ [mag]

cl013obj2 $K_s = 12.883$ [mag] $\Delta K_s = 0.243$ [mag]

cl013obj4 $K_s = 12.186$ [mag] $\Delta K_s = 0.224$ [mag]

cl013ysoc6 $K_s = 11.920$ [mag] $\Delta K_s = 1.539$ [mag]

cl059obj2 $K_s = 12.155$ [mag] $\Delta K_s = 1.098$ [mag]

cl059ysoc6 $K_s = 12.136$ [mag] $\Delta K_s = 0.307$ [mag]

cl059ysoc7 $K_s = 13.479$ [mag] $\Delta K_s = 0.322$ [mag]

dbs93ysoc5 $K_s = 12.201$ [mag] $\Delta K_s = 0.578$ [mag]

dbs93ysoc8 $K_s = 11.347$ [mag] $\Delta K_s = 0.223$ [mag]

dbs100ysoc2 $K_s = 12.737$ [mag] $\Delta K_s = 1.762$ [mag]

dbs100ysoc4 $K_s = 11.525$ [mag] $\Delta K_s = 1.495$ [mag]

dbs100ysoc10 $K_s = 12.000$ [mag] $\Delta K_s = 0.327$ [mag]

dbs130ysoc5 $K_s = 14.944$ [mag] $\Delta K_s = 0.726$ [mag]

Thus, we calculate the mean and standard deviation of stellar ages, masses, temperature and luminosity of YSOs from the adopted models, which are tabulated in Table 5. Only seven stars are fitted, the rest of the objects do not have enough measurements to construct reliable SEDs. As can be seen from the Table 5, six of our sources can be classified as massive young stellar objects, with masses grater that $8M_\odot$, only DBS100 Obj1 is an intermediate-mass objects. All of the objects are very young. The stellar temperatures of the sources are ranging from 4400 to 37000 K. Every SED model shows a presence of envelope. Only for DBS100 Obj1 the presence of a disk is not detected. It's interesting that Cl010 Obj1 is very massive and has a relatively large amplitude of variability (0.49 mag in K_S). Such high variability has rarely been seen in massive YSOs.

6. Summary

In this paper we are reporting some follow-up spectroscopic observations and photometric analysis of eight young stellar clusters projected in the VVV disk area. Using the combination of spectroscopic parallax-based reddening and distance determinations with main sequence and pre-main sequence ishochrone fitting we determine the basic parameters (reddening, age, distance) of the sample clusters. The lower mass limit estimations show that all clusters are low or intermediate mass (between 110 and 1800 $M_\odot$), the slope Γ of
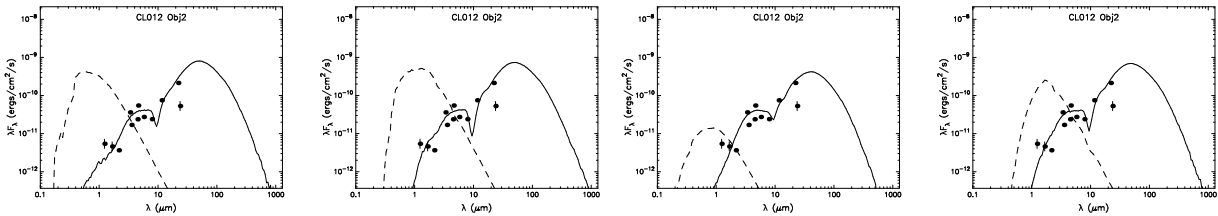
Fig. 17.— Four different SEDs models (solid lines) for the CL 012 Obj2. The dashed line plots the best fit photometric model.

40

the obtained present-day mass functions of the clusters is close to the Kroupa IMF. Using VVV and GLIMPSE color-color cuts we have selected a large number of YSO candidates, which are checked for variability, taking advantage of multi-epoch VVV observations. Fifty seven % of the YSO candidates are found to show at least low-amplitude variability. In few cases it was possible to distinguish between YSO and AGB classification on the basis of the light curves. The SEDs of the spectroscopically confirmed YSO are determined, showing that in general these objects are massive.

Table 5.   The stellar ages, masses, temperature and luminosity of YSOs. Note that the errors are also in logarithmic scale.

Object	Log(Age)	Log(Mass) ($M_\odot$)	Log(T) (K)	Log(Disk Mass) ($M_\odot$)	Log(L_{tot}) ($L_\odot$)	Log(Env. Mass) ($M_\odot$)
CL010 Obj1	4.38±0.09	1.23±0.05	4.32±0.14	-0.65±0.40	4.59±0.19	3.43±0.10
CL012 Obj2	4.14±0.52	0.82±0.31	3.69±0.10	-1.15±0.54	2.94±0.82	1.83±0.61
CL013 Obj1	5.85±0.10	0.91±0.07	4.36±0.04	-3.33±0.65	3.46±0.25	1.17±0.16
CL059 Obj1	3.72±0.13	1.08±0.05	3.66±0.02	-0.26±0.08	3.64±0.25	1.51±0.47
DBS75 Obj1	5.50±0.24	1.35±0.04	4.57±0.01	-2.04±0.54	4.79±0.05	1.79±0.19
DBS93 Obj2	4.81±0.28	0.94±0.04	3.92±0.12	-1.40±0.37	3.35±0.16	2.33±0.69
DBS100 Obj1	5.10±0.18	0.40±0.21	4.16±0.02	-2.18±0.78	1.60±0.20	0.02±0.71

REFERENCES

Alonso-García, J., Dékány, I., Catelan, M., et al. 2015, AJ, 149, 99

Arnaboldi, M., Neeser, M. J., Parker, L. C., et al. 2007, The Messenger, 127,

Baume, G., Carraro, G., & Momany, Y. 2009, MNRAS, 398, 221

Bell, C. P. M., Rees, J. M., Naylor, T., et al. 2014, MNRAS, 445, 3496

Bik, A., Kaper, L., & Waters, L. B. F. M. 2006, A&A, 455, 561

Bonatto, C., & Bica, E. 2010, A&A, 516, A81

Borissova, J., Bonatto, C., Kurtev, R., et al. 2011, A&A, 532, A131

Borissova, J., Chené, A.-N., Ramírez Alegría, S., et al. 2014, A&A, 569, A24

Caratti o Garatti, A., Stecklum, B., Linz, H., Garcia Lopez, R., & Sanna, A. 2015, A&A,
    573, A82

Chené, A.-N., Borissova, J., Bonatto, C., et al. 2013, A&A, 549, A98

Chené, A.-N., Borissova, J., Clarke, J. R. A., et al. 2012, A&A, 545, A54

Chené, A.-N., Ramírez Alegría, S., Borissova, J., et al. 2015, A&A, 584, A31

Cohen, M., & Barlow, M. J. 1980, ApJ, 238, 585

Contreras Peña, C. E. 2015, Ph.D. Thesis,

Contreras Peña, C., Lucas, P. W., Minniti, D., et al. 2016, arXiv:1602.06267

Cooper, H. D. B., Lumsden, S. L., Oudmaijer, R. D., et al. 2013, MNRAS, 430, 1125

Cox, A. N. 2000, Allen's Astrophysical Quantities, 1

Cross, N. J. G., Collins, R. S., Mann, R. G., et al. 2012, A&A, 548, A119

Crowther, P. A., Hadfield, L. J., Clark, J. S., Negueruela, I., & Vacca, W. D. 2006, MNRAS, 372, 1407

Cyganowski, C. J., Whitney, B. A., Holden, E., et al. 2008, AJ, 136, 2391-2412

Davies, B., Figer, D. F., Kudritzki, R.-P., et al. 2007, ApJ, 671, 781

Dutra, C. M., Bica, E., Soares, J., & Barbuy, B. 2003, A&A, 400, 533

Elson, R. A. W., Fall, S. M., & Freeman, K. C. 1987, ApJ, 323, 54

Hanson, M. M., Conti, P. S., & Rieke, M. J. 1996, ApJS, 107, 281

Hanson, M. M., Kudritzki, R.-P., Kenworthy, M. A., Puls, J., & Tokunaga, A. T. 2005, ApJS, 161, 154

Henize, K. G. 1967, ApJS, 14, 125

Henning, T., Schreyer, K., Launhardt, R., & Burkert, A. 2000, A&A, 353, 211

Hervé, A., Martins, F., Chené, A.-N., Bouret, J.-C., & Borissova, J. 2016, New A, 45, 84

Kharchenko, N. V., Piskunov, A. E., Schilbach, E., Röser, S., & Scholz, R.-D. 2013, A&A, 558, A53

Koornneef, J. 1983, A&A, 128, 84

Kroupa, P. 2001, MNRAS, 322, 231

Lejeune, T., & Schaerer, D. 2001, A&A, 366, 538

Liermann, A., Hamann, W.-R., & Oskinova, L. M. 2009, A&A, 494, 1137

Lumsden, S. L., Hoare, M. G., Urquhart, J. S., et al. 2013, ApJS, 208, 11

Martins, F., & Plez, B. 2006, A&A, 457, 637

Martins, F., Schaerer, D., & Hillier, D. J. 2005, A&A, 436, 1049

Martins, L. P., & Coelho, P. 2007, MNRAS, 381, 1329

Mauerhan, J. C., Van Dyk, S. D., & Morris, P. W. 2011, AJ, 142, 40

Mauro, F., Moni Bidin, C., Chené, A.-N., et al. 2013, Rev. Mexicana Astron. Astrofis., 49, 189

Messineo, M., Zhu, Q., Ivanov, V. D., et al. 2014, A&A, 571, A43

Meyer, M. R., Edwards, S., Hinkle, K. H., & Strom, S. E. 1998, ApJ, 508, 397

Minniti, D., Lucas, P. W., Emerson, J. P., et al. 2010, New A, 15, 433

Moisés, A. P., Damineli, A., Figuerêdo, E., et al. 2011, MNRAS, 411, 705

Morales, E. F. E., Wyrowski, F., Schuller, F., & Menten, K. M. 2013, A&A, 560, A76

Mottram, J. C., Hoare, M. G., Lumsden, S. L., et al. 2007, A&A, 476, 1019

von Newmann 1941, The Annals of Mathematical Statistics, Ann. Math. Statist. No.4, 67

Osterloh, M., Henning, T., & Launhardt, R. 1997, ApJS, 110, 71

Ramírez Alegría, S., Borissova, J., Chené, A. N., et al. 2014, A&A, 564, L9

Rayner, J. T., Cushing, M. C., & Vacca, W. D. 2009, ApJS, 185, 289

Rebull, L. M., Stauffer, J. R., Cody, A. M., et al. 2015, AJ, 150, 175

Richards, J. W., Starr, D. L., Brink, H., et al. 2012, ApJ, 744, 192

Robitaille, T. P., Meade, M. R., Babler, B. L., et al. 2008, AJ, 136, 2413

Saito, R., Hempel, M., Alonso-García, J., et al. 2010, The Messenger, 141, 24

Saito, R. K., Hempel, M., Minniti, D., et al. 2012, A&A, 537, A107

Soto, M., Barbá, R., Gunthardt, G., et al. 2013, A&A, 552, A101

Stetson, P. B. 1996, PASP, 108, 851

Straižys, V., & Lazauskaitė, R. 2009, Baltic Astronomy, 18, 19

Urquhart, J. S., Moore, T. J. T., Schuller, F., et al. 2013, MNRAS, 431, 1752

Wallace, L., & Hinkle, K. 1997, ApJS, 111, 445

Walsh, A. J., Bertoldi, F., Burton, M. G., & Nikola, T. 2001, MNRAS, 326, 36

Walsh, A. J., Hyland, A. R., Robinson, G., & Burton, M. G. 1997, MNRAS, 291, 261

Wu, Y., Wei, Y., Zhao, M., et al. 2004, A&A, 426, 503